Stability of Mg-sulfates at −10°C and the rates of dehydration/rehydration processes under conditions relevant to Mars

Alian Wang,[1] J. J. Freeman,[1] I-Ming Chou,[2] and B. L. Jolliff[1]

Received 22 February 2011; revised 13 August 2011; accepted 11 September 2011; published 21 December 2011.

[1] We report the results of low temperature (−10°C) experiments on the stability fields and phase transition pathways of five hydrous Mg-sulfates. A low temperature form of $MgSO_4 \cdot 7H_2O$ (LT-7w) was found to have a wide stability field that extends to low relative humidity (~13% RH at −10°C). Using information on the timing of phase transitions, we extracted information on the reaction rates of five important dehydration and rehydration processes. We found that the temperature dependencies of rate constants for dehydration processes differ from those of rehydration, which reflect differences in reaction mechanisms. By extrapolating these rate constants versus T correlations into the T range relevant to Mars, we can evaluate the possibility of occurrence of specific processes and the presence of common Mg-sulfate species present on Mars in different periods and locations. We anticipate in a moderate obliquity period, starkeyite and LH-$MgSO_4 \cdot H_2O$ should be two common Mg-sulfates at the surface, another polymorph MH-$MgSO_4 \cdot H_2O$ can exist at the locations where hydrothermal processes may have occurred. In polar regions or within the subsurface of other regions, meridianiite (coexisting with water ice, near 100% RH) and LT-7w (over a large RH range) are the stable phases. During a high obliquity period, meridianiite and LT-7w should exhibit widespread occurrence. The correlations of reaction rates versus temperature found in this study imply that dehydration and rehydration of hydrous Mg-sulfates would always be slower than the sublimation and crystallization of water ice, which would be supported by mission observations from Odyssey and by Mars Exploration Rovers.

Citation: Wang, A., J. J. Freeman, I.-M. Chou, and B. L. Jolliff (2011), Stability of Mg-sulfates at −10°C and the rates of dehydration/rehydration processes under conditions relevant to Mars, *J. Geophys. Res.*, *116*, E12006, doi:10.1029/2011JE003818.

1. Introduction

[2] Mg-sulfates have been observed on Mars by orbital remote sensing (e.g., by the OMEGA instrument on Mars Express and the CRISM instrument on the Mars Reconnaissance Orbiter, MRO) [*Arvidson et al.*, 2005; *Gendrin et al.*, 2005; *Murchie et al.*, 2009], with wide distribution and significant abundances. Many of these observed sulfates, especially polyhydrated sulfates, occur in layers that have thicknesses rarely seen in terrestrial deposits, e.g., 200–400 m thick at Aram Chaos, ~2 km thick at Gale Crater, and ~400 m thick at Capri Chasma [*Lichtenberg et al.*, 2008, 2010; *Milliken et al.*, 2009; *Murchie et al.*, 2007; *Roach et al.*, 2007, 2008, 2009a, 2010]. The mineralogical details of these thick deposits are of interest for in-depth investigation by future landed missions (MSL and ExoMars). The environmental conditions that enabled such large deposits and preservation of sulfate layers also need to be understood.

[3] Furthermore, a change in hydration degree of sulfates was implied by mission observation. The dehydration of ferric sulfates was suggested on the basis of a set of Pancam observations by Spirit rover that revealed a temporal color changes of the subsurface salty soils from tens' of centimeter depths at the "Tyrone" site (near Home Plate, at Gusev Crater) after having been excavated and exposed to the Martian surface atmospheric conditions [*Wang et al.*, 2008; *Wang and Ling*, 2011]. The change of hydration degree of Mg-sulfates (e.g., polyhydrated sulfates) was not observed on Mars by CRISM [*Roach et al.*, 2010].

[4] Recent findings of Mg-, Ca- and Fe-sulfates on Mars have reinforced the importance of sulfates in Martian geology, as indicators of past geologic environments, potential hosts for water, and acid sinks. Sulfur cycling, sulfur redox state changes during sulfur cycling, and the effects of S-bearing species as alteration agents for surface and subsurface materials are all important factors in the hydrological and chemical evolution of the martial surface through time.

[1]Department of Earth and Planetary Sciences and the McDonnell Center for the Space Sciences, Washington University in St. Louis, St. Louis, Missouri, USA.
[2]U.S. Geological Survey, Reston, Virginia, USA.

0148-0227/11/2011JE003818

Table 1. Estimated and Measured Relative Humidity (RH) of Six Selected RH Buffer Solutions at −10°C[a]

	Extrapolated From *Greenspan* [1977]		Measured in Freezer at −10.1°C to −11.7°C	
	$f(H_2O)$ (Pa)	RH (%)	RH (%)	$f(H_2O)$ (Pa)
LiBr	29.0	11.3	13.1–15.3	33.5–39.2
LiCl	*	*	21.0–21.7	53.8–55.6
$MgCl_2$	78.3	30.6	45.8–47.8	117.3–122.4
KI	227.0	88.7	84.2–87.0	215.6–222.8
NaCl	246.5	96.3	85.0–88.1	217.7–225.6
KCl	*	*	96.8–98.9	247.9–253.3

[a]An asterisk in a cell indicates the *f*(H2O) or RH value calculated from a *f*(H2O) vs. T correlation having a known and large uncertainty; it is thus not listed in the table.

[5] Until recently, evidence of the sulfur cycle in Martian surface processes has been scarce. Processes and conditions associated with formation, phase transitions, and survival of various sulfates, as well as the role of sulfates in hosting water in equatorial or other regions, are not well understood. A variety of laboratory experiments have been done to try to close this knowledge gap. These experiments have provided information on the stability fields and phase boundaries of various hydrated sulfates and on their phase transition pathways under conditions relevant to Martian surface and subsurface environments [*Ackermann et al.*, 2009; *Altheide et al.*, 2009; *Chevrier and Altheide*, 2008; *Chou et al.*, 2002; *Chou and Seal*, 2003, 2007; *Chipera and Vaniman*, 2007; *Freemen et al.*, 2007a, 2007b; *Freemen and Wang*, 2009; *Grevel and Majzlan*, 2009; *Kong et al.*, 2010, 2011; *Ling et al.*, 2008, 2009; *Ling and Wang*, 2010; *Peterson and Wang*, 2006; *Majzlan et al.*, 2004, 2005, 2006; *Majzlan and Michallik*, 2007; *Tosca et al.*, 2007; *Vaniman et al.*, 2004; *Vaniman and Chipera*, 2006; *Wang et al.*, 2006, 2007, 2009, 2010; *Wang and Ling*, 2011]. Geochemical models and experiments have also provided hypotheses and evidence for the types and rates of cations released from acidic weathering of igneous rocks with compositions similar to those found on Mars and on the secondary evaporite minerals [*Golden et al.*, 2005, 2008; *Peng et al.*, 2010; *Tosca et al.*, 2004, 2007, 2008; *Tosca and McLennan*, 2006; *Zolotov and Mironenko*, 2007]. In addition, calculations have been made on the stability of various hydrous sulfates in the temperature range relevant to the Martian surface and subsurface as a function of latitude and season, based on Viking MAWD experimental results and thermodynamic data [*Suleimenov et al.*, 1986; *Zolotov*, 1989]. The activation energy for the removal of structural water in epsomite ($MgSO_4{\cdot}7H_2O$) was derived from a Temperature-Programmed Dehydration (TPD) experiment monitored by a quadrupole mass spectrometer (QMS) in an ultrahigh vacuum chamber (~10^{-9} torr) in a temperature range of 100–375 K [*McCord et al.*, 2001].

[6] We have been conducting a systematic experimental study of hydrated Mg-sulfates. The purpose of this study is to extend knowledge of the stability fields, phase-transition pathways, and potentially the reaction rates of these hydrous sulfates under conditions relevant to Martian surface/subsurface environments (present and past), to better understand the observed spatial distribution and temporal variations of Martian sulfates. Our approach uses multiple spectroscopic techniques to link the results from laboratory experiments to those from surface exploration and orbital remote sensing of Mars. The techniques that we used include laser Raman spectroscopy, mid-IR attenuated total reflectance (ATR), Vis-NIR diffuse reflectance spectroscopy, and X-Ray diffraction (XRD).

[7] In previous papers we first reported the synthesis of eleven distinct Mg-sulfates, hydrated and anhydrous, crystalline and amorphous, whose identities were confirmed by XRD, and whose Raman spectral patterns were characterized [*Wang et al.*, 2006]. We then reported the stability field and phase-transition pathways of five hydrates of Mg-sulfate (epsomite $MgSO_4{\cdot}7H_2O$, starkeyite $MgSO_4{\cdot}4H_2O$, monohydrate $MgSO_4{\cdot}H_2O$, amorphous $MgSO_4{\cdot}2H_2O$, and anhydrous $MgSO_4$) obtained through dehydration/rehydration experiments in the temperature range of 5 to 50°C, in the relative humidity (RH) range of 6 to 100%, and for reaction durations up to 18,629 h (776 days) [*Wang et al.*, 2006, 2009]. The dehydration pathways of epsomite when mixed with Ca- and Fe-sulfates, and Fe-oxides and Fe-hydroxides were also reported [*Wang et al.*, 2009]. The unique Raman spectral features of each Mg-sulfate obtained in the first study allowed for direct and non-invasive identification of the minerals (sealed in the reaction vial) in the second study on stability fields and phase-transition pathways; especially in mixtures occurring in the intermediate stages of a dehydration/rehydration process.

[8] In section 2 of this paper, we report the results of our latest experiments on the stability fields and phase-transition pathways of five hydrates of Mg-sulfate ($MgSO_4{\cdot}7H_2O$, $MgSO_4{\cdot}4H_2O$, $MgSO_4{\cdot}H_2O$, amorphous $MgSO_4{\cdot}2H_2O$, and $MgSO_4{\cdot}11H_2O$) at −10°C with RH controlled between ~13% and 98% and up to 33,288 h (over 46 months) of reaction time. On the basis of experimental data in the range of 50°C to −10°C, section 3 of this paper presents the determination of ratios of reaction rates at different temperatures of five important dehydration and rehydration processes of Mg-sulfates, and these correlations are further extrapolated into the T range relevant to Martian surface/subsurface environments. Finally, in section 4 of this paper, the ratios of reaction rates at different temperatures (considering only the order of magnitude), combined with knowledge of stability fields of major Mg-sulfate hydrates, are used to predict the most common Mg-sulfate species present on Mars in different periods and locations.

2. Results of Experiments at −10°C for Stability Field Study

[9] Thirty experiments were conducted at −10°C and six RH levels (Table 1), using five hydrous Mg-sulfates as starting phases. They are epsomite $MgSO_4{\cdot}7H_2O$, starkeyite $MgSO_4{\cdot}4H_2O$, monohydrate $MgSO_4{\cdot}H_2O$, amorphous $MgSO_4{\cdot}2H_2O$, and meridianiite $MgSO_4{\cdot}11H_2O$. The details of these samples and the experimental conditions are described in Appendix A. After over 43–46 months of reaction time, 20 experiments at >22% RH among the total of 30 experiments have reached equilibrium, except one, i.e., the experiment begun with LH-1w in $MgCl_2$-H_2O RH buffer (Table 2). The other 10 experiments at ≤22% RH are still approaching equilibrium as of this writing. Table 2 lists the phases identified by their Raman spectra at intermediate stages of reaction and the apparent final phases of

Table 2. Mg-Sulfate Phases Identified by Raman Spectroscopy in the Products of the Intermediate Stages of Thirty Experiments Conducted at Six RH Levels and −10°C[a]

Starting Material	Duration (hours)	Humidity Buffers					
		LiBr	LiCl	$MgCl_2$	KI	NaCl	KCl
$MgSO_4·H_2O$ (LH-1w)	0	LH-1w	LH-1w	LH-1w	LH-1w	LH-1w	LH-1w
	288	LH-1w	LH-1w	LH-1w	LT-7w>1w	LT-7w>1w	LT-7w>1w
	504	LH-1w	LH-1w	LH-1w, trLT-7w	LT-7w	LT-7w	LT-7w
	1656	LH-1w	LH-1w	LH-1w > LT-7w	LT-7w	LT-7w	11w>LT-7w
	2520	LH-1w	LH-1w	LH-1w, trLT-7w	LT-7w	LT-7w	11w>LT-7w
	4320	LH-1w	LH-1w	LT-7w	LT-7w	LT-7w	11w
	6528	LH-1w	LH-1w	LT-7w, 1w	LT-7w	LT-7w	11w
	10704	LH-1w	LH-1w	LT-7w	LT-7w	LT-7w	11w
	12384	LH-1w	LH-1w, 2wtr	LT-7w, 1w	LT-7w	LT-7w	11w
	15576	LH-1w	LH-1w	LT-7w, 1w	LT-7w	LT-7w	11w
	29256	LH-1w	LH-1w	LT-7w, 1w	LT-7w	LT-7w	11w
	33192	LH-1w	LH-1w	LT-7w, 1w	LT-7w	LT-7w	11w
Am. $MgSO_4·2H_2O$	0	Am	Am	Am	Am	Am	Am
	288	Am	Am	Am > LT-7w	LT-7w	LT-7w	LT-7w
	504	Am	Am	Am > LT-7w	LT-7w	LT-7w	LT-7w
	1656	Am	Am	LT-7w	LT-7w	LT-7w	11w
	2520	Am	Am	LT-7w	LT-7w	LT-7w	11w
	4320	Am,7wtr	Am,7wtr	LT-7w	LT-7w	LT-7w	11w
	6528	Am,7wtr	Am,7wtr	LT-7w	LT-7w	LT-7w	11w
	10704	Am,7wtr	Am,7wtr	LT-7w	LT-7w	LT-7w	11w
	12384	Am,7w	Am,7w	LT-7w	LT-7w	LT-7w	11w
	15576	Am,7w	Am,7w	LT-7w	LT-7w	LT-7w	11w
	29256	Am,7w	Am,7w	LT-7w	LT-7w	LT-7w	11w
	33192	Am,7w	Am,7w	LT-7w	LT-7w	LT-7w	11w
$MgSO_4·4H_2O$	0	4w	4w	4w	4w	4w	4w
	288	4w	4w	4w	LT-7w	LT-7w	LT-7w
	504	4w	4w	4w>LT-7w	LT-7w	LT-7w	LT-7w
	1656	4w	4w	LT-7w>4w	LT-7w	LT-7w	LT-7w+11w
	2520	4w	4w	LT-7w	LT-7w	LT-7w	11w, trLT-7w
	4320	4w	4w	LT-7w	LT-7w	LT-7w	11w
	6528	4w	4w	LT-7w	LT-7w	LT-7w	11w
	10704	4w	4w	LT-7w	LT-7w	LT-7w	11w
	12384	4w	4w	LT-7w	LT-7w	LT-7w	11w
	15576	4w	4w	LT-7w	LT-7w	LT-7w	11w
	29256	4w	4w	LT-7w	LT-7w	LT-7w	11w
	33192	4w	4w	LT-7w	LT-7w	LT-7w	11w
$MgSO_4·7H_2O$	0	7w	7w	7w	7w	7w	7w
	288	LT-7w	LT-7w	LT-7w	LT-7w	LT-7w	LT-7w
	504	LT-7w	LT-7w	LT-7w	LT-7w	LT-7w	LT-7w
	1656	LT-7w	LT-7w	LT-7w	LT-7w	LT-7w	LT-7w>11w
	2520	LT-7w	LT-7w	LT-7w	LT-7w	LT-7w	11w
	4320	LT-7w	LT-7w	LT-7w	LT-7w	LT-7w	11w
	6528	LT-7w	LT-7w	LT-7w	LT-7w	LT-7w	11w
	10704	LT-7w	LT-7w	LT-7w	LT-7w	LT-7w	11w
	12384	LT-7w	LT-7w	LT-7w	LT-7w	LT-7w	11w
	15576	LT-7w	LT-7w	LT-7w	LT-7w	LT-7w	11w
	29352	LT-7w	LT-7w	LT-7w	LT-7w	LT-7w	11w
	33288	LT-7w	LT-7w	LT-7w	LT-7w	LT-7w	11w
$MgSO_4·11H_2O$	0	11w	11w	11w	11w	11w	11w
	144	LT-7w	LT-7w	11w	LT-7w>11w	11w	LT-7w>11w
	1008	LT-7w	LT-7w	LT-7w	11w>LT-7w	11w>LT-7w	11w>>LT-7w
	2520	LT-7w	LT-7w	LT-7w	LT-7w, 11w	11w, LT-7w	11w>>>LT-7w
	4728	LT-7w	LT-7w	LT-7w	LT-7w	LT-7w	11w
	8904	LT-7w	LT-7w	LT-7w	LT-7w	LT-7w	11w
	10584	LT-7w	LT-7w	LT-7w	LT-7w	LT-7w	11w
	13776	LT-7w	LT-7w	LT-7w	LT-7w	LT-7w	11w
	27552	LT-7w	LT-7w	LT-7w	LT-7w	LT-7w	11w
	31488	LT-7w	LT-7w	LT-7w	LT-7w	LT-7w	11w

[a]The results are presented separately for five starting Mg-sulfate phases. These experiments lasted for 43–46 months. Phase identifications made at intermediate stages reveal the development of equilibrium and the pathway of a phase-transition. Note the experiments with meridianiite as starting phase were started later than the other 24 experiments.

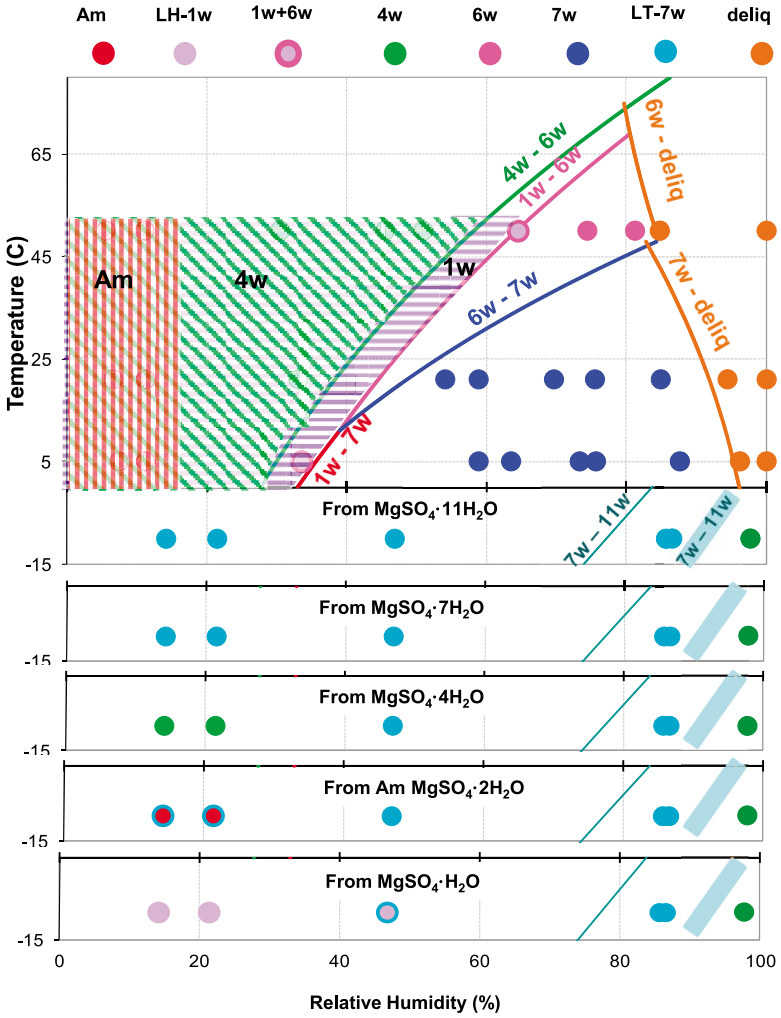

Figure 1. The final phases of Mg-sulfates from 30 experiments at −10°C are shown in five plots of data points below 0°C. Each plot corresponds to a different starting phase (marked in that plot). The phase identifications (annotated by colored circles) were made on the basis of their Raman spectra. The phase boundary lines of 4w-6w, 1w-6w, 6w-7w, 1w-7w, 6w-deliq, 7w-deliq, and 7w-11w are from *Chou and Seal* [2003, 2007]. The location of the second 7w-11w phase boundary (shown as a wide zone in each of five plots below 0°C) is based on the observations of this study. The results at −10°C are compared with the results of experiments at 5, 21, and 50°C (three rows of data points above 0°C from the 120 experiments reported by *Wang et al.* [2009]). The shadowed areas above 0°C (marked as Am, 4w, and 1w) indicate the overlaps of stability/metastability fields of these three phases. Annotation: Am, amorphous $MgSO_4{\cdot}2H_2O$; LH-1w, $MgSO_4{\cdot}H_2O$ formed at low RH; 4w, $MgSO_4{\cdot}4H_2O$; 6w, $MgSO_4{\cdot}6H_2O$; 7w, $MgSO_4{\cdot}7H_2O$; LT-7W, low temperature form of $MgSO_4{\cdot}7H_2O$; deliq, deliquescence of solid Mg-sulfates.

Mg-sulfates at the end of 31,488–33,288 h of reaction time. The phase transition pathways were inferred by these phase IDs.

[10] The final phases of Mg-sulfates in 30 experiments at −10°C are compared in Figure 1 with the stable phases in the experiments at 5°C, 21°C, and 50°C [*Wang et al.*, 2009]. The results from five different starting phases of this study are shown separately in five plots below 0°C (Figure 1). These observed final phases were plotted against the known phase boundaries for hydrated Mg-sulfates (6w-7w from *Chou and Seal* [2003], 4w-6w and 1w-7w from *Chou and Seal* [2007]). Among these phase boundaries, the 11w-7w phase boundary below 0°C was predicted [*Chou and Seal*, 2007]. In the following sections, we describe the major results from these experiments.

2.1. Higher Than Predicted $f(H_2O)$ Stability for Meridianiite (11w) at −10°C

[11] All five starting phases in the KCl-H_2O RH buffer converted to meridianiite (11w). In contrast, all five starting phases in the NaCl-H_2O buffer converted to an Mg-sulfate phase with seven structural waters but with a slightly distorted structure from standard epsomite $MgSO_4{\cdot}7H_2O$ (the details of this phase, LT-7w, are discussed in section 2.2). These observations suggest that at −10°C, an 11w-7w phase boundary passes through a point between the two RH values

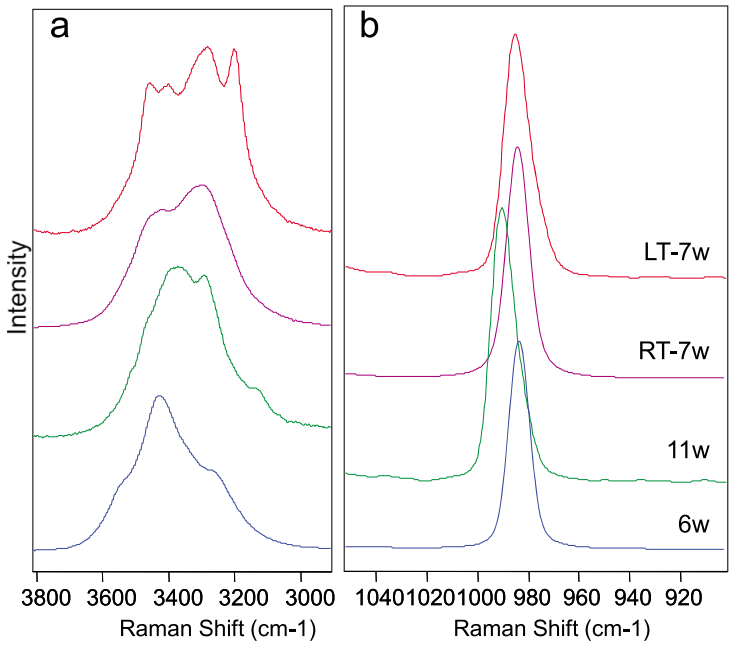

Figure 2. Raman spectra of LT-7w (recorded at −78.5°C) found in the final products of experiments at −10°C, in comparison with Raman spectra of epsomite (RT-7w), hexahydrite (6w), and meridianiite (11w). (a) Spectral region for H_2O vibrational modes. (b) Spectral region for symmetric-stretching vibrational mode of $[SO_4]^{2-}$ tetrahedra.

fixed by KCl- and NaCl-saturated aqueous solutions (see section A2, RH values of binary salt-H_2O humidity buffers at −10°C).

[12] The prediction of the 11w-7w phase boundary by *Chou and Seal* [2007] suggests that it intersects with the −10°C isotherm at $f(H_2O)$ of 200.5 Pa, corresponding to an RH value of 77.24% (shown in Figure 1). This prediction was based on (1) an observation of the stability of meridianiite ($MgSO_4{\cdot}11H_2O$) (which melts at 2°C [*Peterson and Wang*, 2006]), (2) a calculation of $\alpha(H_2O)$ (activity of H_2O) using Pitzer's model, and (3) thermodynamic reasoning that the enthalpy for adding additional water molecules to a hydrous Mg-sulfate structure is constant (−297.77 kJ mol^{-1}) after forming hexahydrite ($MgSO_4{\cdot}6H_2O$) [*Chou and Seal*, 2007, Appendix A], because the additional structural water molecules do not bond to either SO_4 tetrahedra or $Mg(OH_2)_6$ octahedra.

[13] In our experiments, all five starting phases converted to LT-7w at −10°C and a RH value buffered by NaCl-saturated aqueous solution, whose measured RH range (85.0–88.1%, Table 1) are much higher than the 77.24% RH predicted by *Chou and Seal* [2007] for the 11w-7w phase boundary at −10°C. This discrepancy can be caused by the uncertainty associated with the position of the isobaric invariant point at 2°C and 95.77% RH for the coexistence of 7w, 11w, and the aqueous phase used by *Chou and Seal* [2007] to make their prediction. Fundamentally, this discrepancy can only be solved by the experimental determination of the water vapor pressure of the RH buffers using saturated aqueous solutions of binary salts below 0°C.

[14] Nevertheless, our observations from the experiments using KCl-H_2O and NaCl-H_2O buffers confirmed that at −10°C, the 11w-7w phase boundary passes a point in the RH zone (Figure 1) defined by the RH values of NaCl- and KCl-saturated aqueous solutions on each side. This result means that not only will meridianiite ($MgSO_4{\cdot}11H_2O$) be stable when coexisting with ice (i.e., at or near 100% RH), but more importantly, it will convert readily to LT-7w with a 5–10% decrease of $f(H_2O)$ at −10°C (Tables 1 and 2).

2.2. Stable $MgSO_4{\cdot}7H_2O$ (LT-7w) in the Mid-RH Zone at −10°C

[15] In the mid-RH zone buffered by the saturated aqueous solutions of $MgCl_2$, KI, and NaCl at −10°C (measured RH ~46–88% in Figure 1 and Table 1), all five starting phases converted to a phase that possesses a Raman spectral pattern (marked as LT-7w in Figure 2) different from the Raman spectrum of epsomite, the structural form of $MgSO_4{\cdot}7H_2O$ above 0°C (labeled as RT-7w in Figure 2). In addition, during the conversion of 1w, 4w, and Am to meridianiite (11w) in the KCl-H_2O buffer at −10°C ("KCl" column of Table 2), all of these phases converted to LT-7w first, then to 11w, i.e., LT-7w is an intermediate phase along the pathway for their phase transition to 11w at low temperature (≤−10°C) (Table 2).

[16] We have found that the occurrence of this LT-7w can be easily reproduced by storing epsomite powders in a sealed sample vial at −10°C for a few days. In addition, the gravimetric analyses before and after heating of this sample at 400°C confirmed that it has 7 structural water molecules per formula unit.

2.2.1. Raman Spectral Evidence for LT-7w

[17] The Raman spectrum of LT-7w is directly compared with that of a normal epsomite (RT-7w) in Figure 2. Spectra of hexahydrite (6w) and meridianiite (11w) are also shown in Figure 2 in order to confirm that neither dehydration (to 6w) nor rehydration (to 11w) occurred during the formation of LT-7w. We found that the major spectral differ-

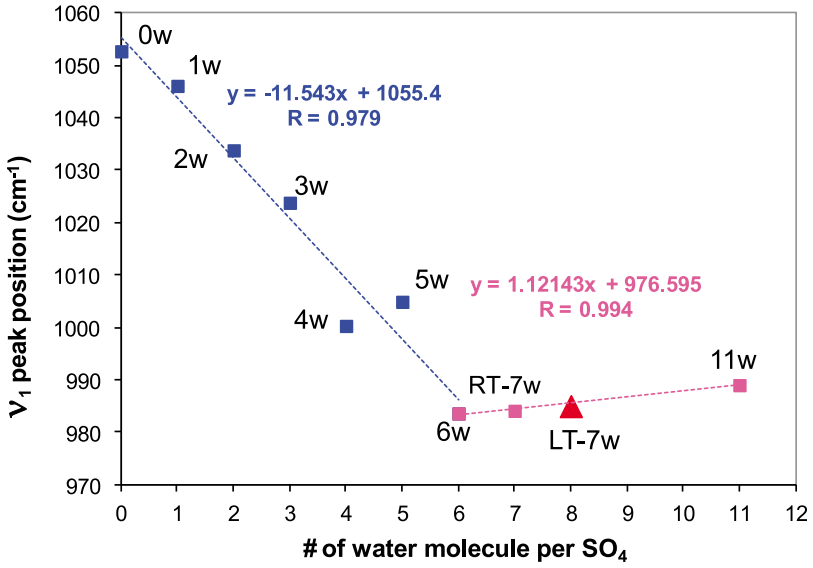

Figure 3. Two opposite trends of Raman ν_1^{SO4} peak shift that represent the change of structural roles of water molecules in Mg-sulfates.

ences between the two heptahydrates of magnesium sulfates (RT-7w and LT-7w) occur in the 3000–3800 cm^{-1} spectral region (Figure 2a), where the fundamental symmetric (ν_1^{H2O}) and asymmetric stretching (ν_3^{H2O}), and secondary overtone of bending vibrational modes ($2\nu_2^{H2O}$) of structural water occur. Four well-resolved Raman peaks (3459, 3404, 3286, 3203 cm^{-1}) appear in the LT-7w spectrum, compared with the two peaks (3425, 3303 cm^{-1}) in the spectrum of epsomite (RT-7w). Furthermore, the center of the envelope that encloses multiple peaks of LT-7w shifts ($\Delta\nu_{shift}$ ~20 cm^{-1}) to lower wavenumber from that of epsomite. For comparison, the peak envelope centers for meridianiite and hexahydrite shift to high wavenumber, $\Delta\nu_{shift}$ ~10 cm^{-1} and ~80 cm^{-1}, respectively.

[18] In the spectral region of LT-7w at 970–1000 cm^{-1} (Figure 2b), where the fundamental symmetric stretching mode (ν_1^{SO4}) of the SO_4 tetrahedron occurs, the Raman ν_1 peak of LT-7w shifts slightly to higher wavenumber ($\Delta\nu_{shift}$ ~0.9 cm^{-1}) from the ν_1 peak position of epsomite (RT-7w). It also has an increased peak width ($\Delta\nu_{FWHH}$ ~11.7cm^{-1}) compared with that of the epsomite peak width ($\Delta\nu_{FWHH}$ ~10.7 cm^{-1}). Meridianiite (11w) also has its ν_1 peak shifted to higher wavenumber ($\Delta\nu_{shift}$ ~6.2 cm^{-1}) from the epsomite ν_1 peak. This trend of peak shifts to higher wavenumber with increase in the degree of hydration is in the opposite direction compared to the trend of shifts to lower wavenumber observed with increase in the degree of hydration from anhydrous (0w) to hexahydrite (6w) of Mg-sulfates (Figure 3, based on the work of *Wang et al.* [2006] and this study).

[19] We think there is a structural reason for the two different trends of ν_1^{SO4} peak-shift. The water molecules added into the structure of anhydrous Mg-sulfate (0w), monohydrate (1w), sanderite ($MgSO_4{\cdot}2H_2O$), $MgSO_4{\cdot}3H_2O$, starkeyite (4w), pentahydrate (5w), and hexahydrite (6w) are linked to Mg to form $[Mg(O,OH_2)_6]$ octahedra. Hydrogen bonding between the H atoms of water in $[Mg(O,OH_2)_6]$ octahedra and the O atoms in SO_4 tetrahedra will shorten the bonds among polyhedra but lengthen the S-O bond in SO_4 tetrahedra. Thus additional water would induce a weaker S-O stretching vibration causing ν_1^{SO4} peak shifts to lower wavenumber. Once the six corners of a Mg-octahedron are completely occupied by "OH_2" forming ($[Mg(OH_2)_6]$) in hexahydrite, the additional water to form epsomite (and further to form meridianiite) would only occupy the spaces among SO_4 tetrahedra and $Mg(OH_2)_6$ octahedra as interstitial water. Thus additional water would have the effect of pushing polyhedra away from each other, which, in turn, would actually tighten the affected SO_4 tetrahedra so as to shorten S-O bonds and strengthen the S-O stretching vibration (causing ν_1^{SO4} peak shifts to higher wavenumber). Therefore, it is the difference in the structural function of water molecules (interstitial water versus octahedral OH_2) that causes the opposite trends of Raman ν_1^{SO4} peak shifts. Hexahydrite marks the turning point in this trend (Figure 3).

[20] Based on the method of synthesizing LT-7w and the gravimetric measurements before and after heating at 400°C of LT-7w, we confirmed that only seven water molecules per SO_4 exist in the LT-7w structure. The fact that the ν_1^{SO4} peak position of LT-7W falls in the middle of the trend of shifts to higher wavenumbers mentioned above (Figure 3) can be interpreted using the same principle, i.e., the slight shift of the LT-7w ν_1^{SO4} peak indicates a minor increase (from RT-7w) of inter-polyhedral distances in the LT-7w structure. This minor increase of inter-polyhedral distances, at low temperature, can be introduced by slightly adjusted the positioning of interstitial water molecules among the polyhedra. The observation in the 3000–3800 cm^{-1} Raman spectral region supports this hypothesis: the appearance of four narrow water peaks in this spectral region of LT-7w suggests the formation of additional crystallographically distinct H_2O sites in its structure at low temperature. Note that the ν_1^{SO4} peak position of LT-7W plotted in Figure 3 is only a demonstration of slightly increased inter-polyhedral distance, not an indication of an Mg-sulfate with eight structural waters.

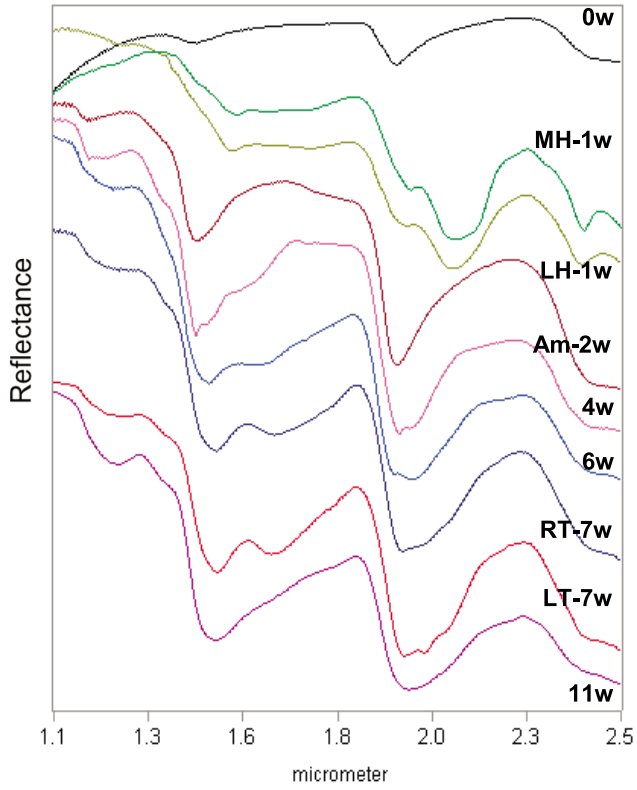

Figure 4. Near Infrared (NIR) reflectance spectra (1.1–2.5 μm) of Mg-sulfates with different degrees of hydration (spectra were shifted vertically to show the detailed spectral features). Compared with that of RT-7w, the NIR spectrum (red color) of LT-7w shows better resolved peaks in the 1.4–1.7 μm range, with a stronger 1.6 μm peak, and three fine spectral features in the 1.9–2.2 μm range. Its NIR spectrum is very distinct from the spectra of other hydrous Mg-sulfates. The peaks seen in the spectrum of 0w are from adsorbed water.

2.2.2. NIR Spectral Evidence for LT-7w

[21] Among the NIR (1.1 to 2.5 μm region) reflectance spectra of Mg-sulfates [*Altheide et al.*, 2009; *McCord et al.*, 2001; this study] from anhydrous (0w) to meridianiite (11w) (Figure 4), three systematic trends of band shifts are observed following the increase of hydration degree, as follows: a red shift from the 1.168 μm band of amorphous (2w) to 1.250 μm band of meridianiite (11w), a red shift from the 1.434 μm band of anhydrous (0w) to 1.487 μm band of meridianiite (11w), and a red shift from the 1.933 μm band of anhydrous (0w) to 1.963 μm band of meridianiite (11w). The spectral patterns of monohydrates are quite different from other Mg-sulfates. The spectra of MH-1w and LH-1w (structural details discussed by *Wang et al.* [2009]) have a similar spectral pattern, but four trends of blue shifts are observed from MH-1w to LH-1w, from 1.543 to 1.528 μm, 1.967 to 1.956 μm, 2.084 to 2.068 μm, and 2.399 to 2.391 μm. In addition, a band of MH-1w near 2.08 μm has a flatter top than that of LH-1w. Note these minor differences in spectral features that distinguishing MH-1w from LH-1w may not be resolvable in Mars orbital remote sensing NIR spectra because of the typically low S/N.

[22] Figure 4 shows that in NIR reflectance spectra, the double peaks of LT-7w in the 1.4–1.7 μm region are better resolved than those in the epsomite spectrum (marked as RT-7w), with an increased intensity of the second peak near 1.6 μm. In addition, LT-7w shows three fine spectral features in 1.9–2.2 μm region that are not observed in the epsomite spectrum (Figure 4). These features make NIR spectrum of LT-7w to be very distinct from the spectra of other hydrous Mg-sulfates. The spectral peaks in the 1.1–2.5 μm NIR region are the overtone and combinational modes of fundamental vibrational modes of structural water in Mg-sulfate structures. A set of better resolved spectral features in the NIR spectral region of LT-7w is consistent with the appearance of multiple, sharp Raman peaks of LT-7w in the 3000–3800 cm^{-1} region that contains mainly the fundamental vibrational modes of structural water (Figure 2a).

[23] The NIR spectral pattern of meridianiite (11w) in the 1.1–2.5 μm region (Figure 4) differs also from all other Mg-sulfates (from 1w to 7w). It has lost all detailed spectral features in the spectral region of ~1.4 μm, 1.9 μm, and 2.4 μm. It also has a much larger band width than the spectral band near 1.9 μm of 2w, 4w, 6w, 7w, and LT-7w. The band-broadening and loss of fine spectral features in the spectrum of 11w could be caused by the presence of the five interstitial water molecules occurring in the spaces among octahedra and tetrahedra in its structure.

2.2.3. X-Ray Diffraction Evidence for LT-7w

[24] Five batches of LT-7w samples were analyzed using the specially designed low-T XRD sample holder at CO_2 ice temperature. Scans were taken from 14° to 44° 2θ using 0.04° steps and 1s dwell time. After each scan, the XRD sample holder was checked to confirm that dry ice grains remained in the ice box (i.e., T = −78.5°C was maintained), indicating that no phase transition should have occurred. The fifth batch of the LT-7w sample was kept at room temperature for >30 min, then the final XRD scan was taken on the same sample using exactly the same measurement parameters. This experiment confirmed that the LT-7w sample was totally converted back to epsomite (RT-7w).

[25] Figure 5a shows the XRD pattern of LT-7w compared with the XRD pattern of epsomite (RT-7w) obtained from the final XRD scan. When considering some closely occurring lines as line-groups, it appears that in two XRD patterns, there are similar numbers of line-groups, they occur at similar 2θ locations, and they have similar relative intensities. One of the differences is that there are more lines in each line-group of the LT-7w XRD pattern. For example, among the four line-groups with $2\theta < 22°$ in the LT-7w XRD pattern (Figure 5b), there are four lines near 14.8°, three lines near 16.5°, two lines near 19.7°, and three lines near 21.3°, whereas in the RT-7w XRD pattern, there are only two lines near 14.8°, two lines near 16.5°, one line near 19.7°, and one line near 21.3°. The second difference is that the lines (within line-groups) in the LT-7w XRD pattern shift generally toward higher 2θ values. This general line-shift trend suggests a reduction of unit-cell size, probably resulting from thermal contraction, consistent with the fact that LT-7w is a low-temperature phase. The third difference is the appearance of some lines in the region of $2\theta > 30°$.

[26] The splitting of each line-group into more XRD lines could be caused by differential contraction along the different crystallographic axes of the unit cell in LT-7w. There

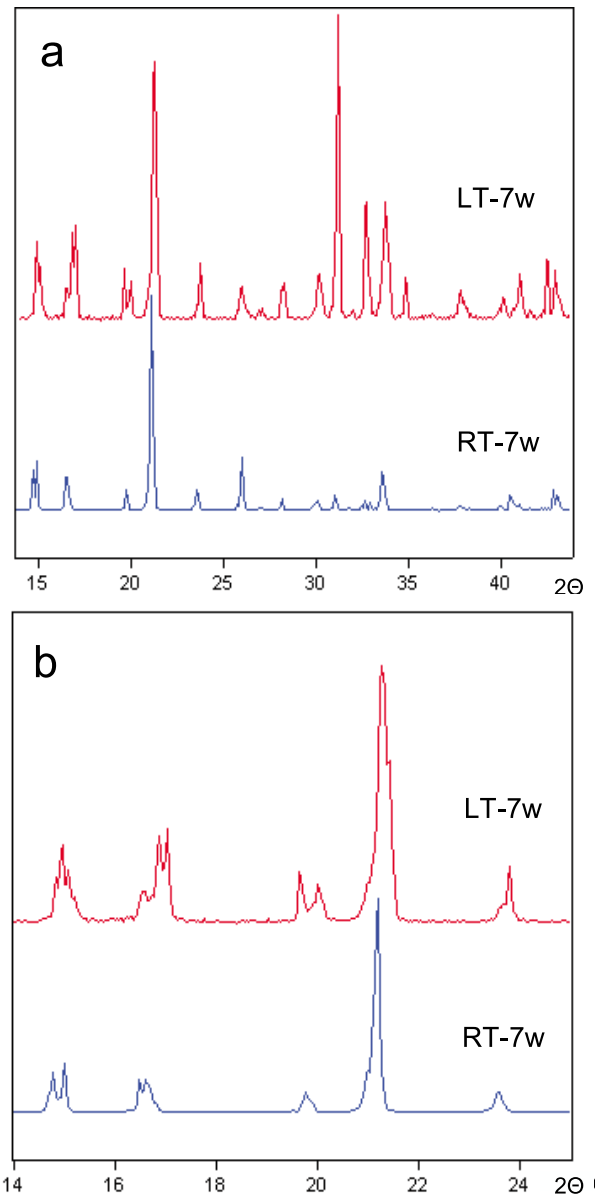

Figure 5. XRD pattern of LT-7w compared to that of RT-7w. Both measurements were made using the same specially designed XRD sample holder and the same parameters, except that LT-7w sample was measured at the temperature of dry ice (−78.5°C), whereas the RT-7w sample was the last batch of the LT-7w sample, measured at room temperature ~30 min after the LT-7w XRD measurement was completed. (a) The 2θ range of 14°–45°. (b) The 2θ range of 14°–25°.

is some evidence from observations in the literature suggesting that sulfate hydrates form lower-symmetry structures at reduced temperature. For example, an orthorhombic to monoclinic transformation of sodium ammonium sulfate dehydrate, from $P2_12_12_1$ to $P2_1$, was reported by *Lipiński et al.* [2001]. In addition, a powder neutron diffraction study of $MgSO_4{\cdot}7D_2O$ in the 1.8–300 K temperature range [*Fortes et al.*, 2006] concluded that a similar orthorhombic to monoclinic transformation could not be excluded, evidenced especially by a significant reduction of angle β from 90°. Furthermore, using the unit cell parameters of $MgSO_4{\cdot}7D_2O$ at low temperature [*Fortes et al.*, 2006], the splitting of XRD line-groups near 14.8° (002, 101, 110) and near 16.5° (012, 111, 021) were reproduced (as we observed in the LT-7w XRD pattern) in a calculated XRD pattern (R. Peterson, personal communication, 2010). This line splitting appears to bear a correspondence with the extra spectral components in the OH region of the Raman spectrum (Figure 2a) and in the NIR reflectance spectrum (Figure 4).

[27] The results from XRD, Raman, and NIR spectroscopy all suggest that LT-7w has a slightly distorted crystal structure relative to the orthorhombic structure ($P2_12_12_1$) of normal epsomite (RT-7w). The importance of this structurally distorted heptahydrate magnesium sulfate (LT-7w) is that it has a very wide stability field at low temperature and in mid- to low-RH regions, and it is the middle phase during the rehydration of kieserite, starkeyite, and amorphous Mg-sulfates at low temperature to form meridianiite.

2.3. Expansion of Stability Field of LT-7w Into Low RH Range at −10°C

[28] After over 46 months of dehydration in LiBr-H_2O and LiCl-H_2O RH buffers at −10°C (measured RH ≤ 22%, Table 1), starkeyite (4w) and LH-1w remained unchanged (third and fifth plots below 0°C in Figure 1 and in the "LiBr" and "LiCl" columns in Table 2) suggesting that these two species are stable or metastable in the tested T-RH ranges. The final starkeyite phase shows a well-resolved five peak-pattern (3329.6, 3396.3, 3425.4, 3485.6, and 3557.8 cm^{-1}) in the H_2O spectral range (3800–2900 cm^{-1}, Figure 6a), whereas the same peaks (same peak positions and relative peak intensities) of RT-4w overlap with each other. The position of ν_1^{SO4} peak (at 1000.6 cm^{-1}) of starkeyite at −10°C shows a minor up-shift from that of RT-4w (at 999.9 cm^{-1}) that is consistent with a reduction of unit-cell size caused by low temperature (Figure 6b), whereas no indication of real structural change as in LT-7w was found (Figures 2 and 5).

[29] In LiBr-H_2O and LiCl-H_2O RH buffers at −10°C (measured RH 13–22%), both meridianiite (11w) and epsomite (7w) converted to LT-7w (first and second plots below 0°C in Figure 1 and in the "LiBr" and "LiCl" columns in Table 2). More importantly, amorphous $MgSO_4{\cdot}2H_2O$ (Am) in LiBr-H_2O and LiCl-H_2O RH buffers at −10°C show evidence of gradual development of a transition to a heptahydrate phase starting from 4320 h (the "LiBr" and "LiCl" columns in the "Am. $MgSO_4{\cdot}2H_2O$" section of Table 2 and in the fourth plot below 0°C in Figure 1). This gradually developing phase transition is demonstrated in Figure 7 as a sharp Raman peak near 985.3 cm^{-1} (of 7w) appears next to a broad Raman peak centered at 1030 cm^{-1} of amorphous $MgSO_4{\cdot}2H_2O$. This sharp peak gradually increases its intensity following the increase of time duration in LiBr-H_2O and LiCl-H_2O RH buffers at −10°C (13–22% RH). Unfortunately, a high background in the Raman spectrum developed during the phase transition prevents a definitive identification of the new heptahydrate phase between epsomite (RT-7w) and LT-7w by using the Raman spectral features in the range 3000–3800 cm^{-1}. Nevertheless, based on the conversion of epsomite (RT-7w) to LT-7w under the same experimental conditions (the "LiBr" and "LiCl" columns in the "$MgSO_4{\cdot}7H_2O$" section of Table 2 and in the

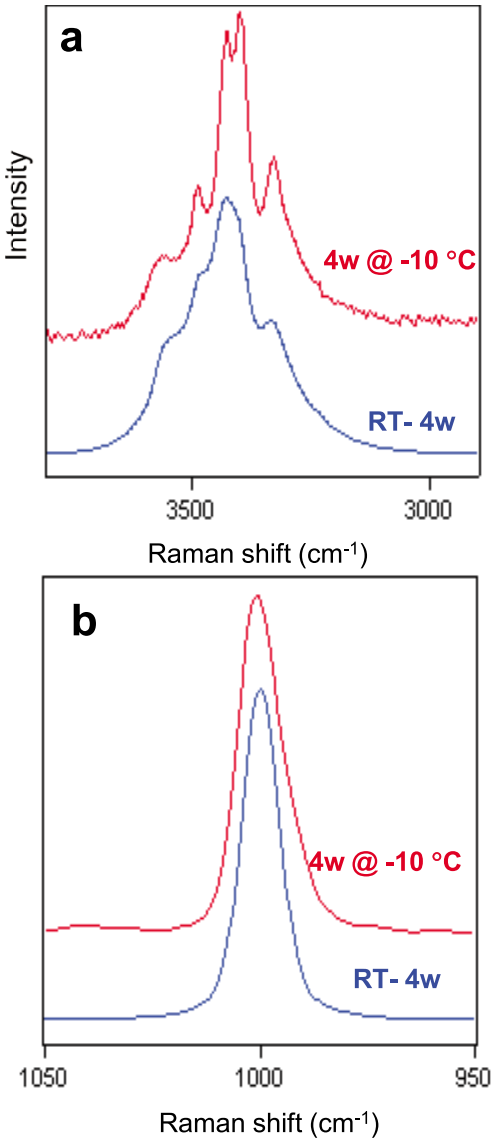

Figure 6. Raman spectra of starkeyite from experiments in LiBr and LiCl RH buffers at −10°C. Spectra are compared with those of starkeyite at room temperature (RT-4w). (a) Vibrational modes of structural water. (b) Vibrational mode of SO_4 tetrahedra.

second plot below 0°C in Figure 1), we anticipate that the magnesium sulfate heptahydrate phase converted from Am should have the LT-7w structure.

[30] The phase transition of Am at −10°C differs from those above 0°C (e.g., T ~5°C ± 1°C) reported previously [*Wang et al.*, 2009]. The same Am samples ($MgSO_4{\cdot}2H_2O$) were stable in LiBr-H_2O and LiCl-H_2O RH buffers (7.4% < RH < 11.3%) at 5°C ± 1°C for 17,616 h (734 days) [*Wang et al.*, 2009, Table 5], and their stabilities were further confirmed by a recent measurement for even longer duration (after 23016 h, 959 days). The new experiments at −10°C demonstrate a reduction of the stability field of the Am phase at low T. Furthermore, the new experiments show a change in the rehydration pathway of Am, i.e., from Am to LT-7w, whereas in 5°C ≤ T ≤ 50°C with RH ≥ 31%, the Am samples always first converted to starkeyite (4w), then to mixtures of 4w, 5w, 6w, 7w, and finally deliquescence occurred [*Wang et al.*, 2009, Table 5]. At −10°C, no starkeyite (4w) was identified at any intermediate stages of Am rehydration experiments (the "Am. $MgSO_4{\cdot}2H_2O$" section of Table 2), indicating that the phase transition Am→ 7w is favored at this temperature.

[31] An additional significance of this observation is that it suggests an extended stability field of LT-7w below 0°C, and with a RH range larger than was suggested by *Chou and Seal* [2007] (1w-7w and 4w-7w boundaries in their Figure 6). Additional support for this argument is that both epsomite (RT-7w) and meridianiite (11w) converted to LT-7w at −10°C under low RH (13% < RH < 22%) (first and second plots below 0°C in Figure 1). One may argue that the slow kinetics at low temperature can be the reason for no further *dehydration* of the LH-7w occurred in these four low RH experiments, whereas the *rehydration* of amorphous Mg-sulfate ($MgSO_4{\cdot}2H_2O$) to LT-7w in the same T-RH range (fourth plot below 0°C in Figure 1) can only indicate an extended stability field of LT-7w to low RH values under low-T condition.

[32] A wide stability field of LT-7w at low T is an important factor for understanding the current Mg-sulfate species on Mars, especially in the subsurface and in the polar regions.

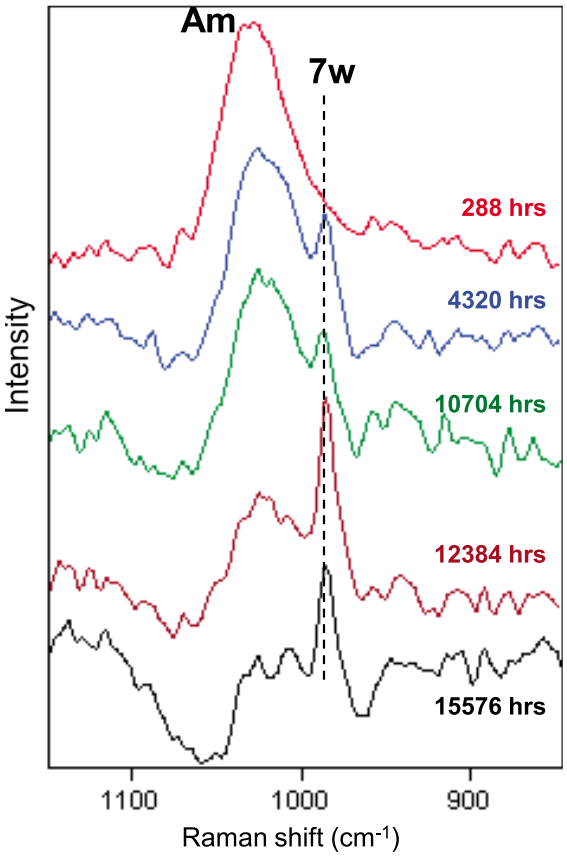

Figure 7. Raman spectral evidence for the development of a phase transition from an amorphous Mg-sulfate ($MgSO_4{\cdot}2H_2O$) to a heptahydrated Mg-sulfate ($MgSO_4{\cdot}7H_2O$), obtained from the intermediate products of two experiments in LiBr-H_2O and LiCl-H_2O RH buffer solutions at −10°C.

For example, during the seasonal change in Martian polar regions when water ice sublimates, the coexisting meridianiite ($MgSO_4 \cdot 11H_2O$) should convert to LT-7w as it requires only 5–10% decrease of $f(H_2O)$ at −10°C (Tables 1 and 2). The observations listed in Table 2 indicate that the 11w → LT-7w conversions are not rapid for a 5–10% decrease of $f(H_2O)$ at −10°C (<4728 h in NaCl-H_2O RH buffer), whereas the conversion can be almost instantaneous for 87% decrease of $f(H_2O)$ even at −10°C (<144 h in LiBr-H_2O and LiCl-H_2O RH buffers). These observations indicate that LT-7w would be one of the two most common hydrated Mg-sulfates (meridianiite would be another) at temperatures ≤−10°C on Mars, including subsurface and polar regions. Section 4 has a more detailed discussion of this issue.

3. Rates of Dehydration and Rehydration of Mg-Sulfates

[33] The types of Mg-sulfates that exist on Mars (surface, subsurface, and polar regions) are not only determined by their stability fields and phase-transition pathways under Martian conditions, but are also affected by the reaction rates of specific dehydration and rehydration processes. The selection of five dehydration and rehydration processes for this study was based on previous studies on Mg-sulfate phase transitions under conditions relevant to Mars [*Chou and Seal*, 2003, 2007; *Chipera and Vaniman*, 2007; *Peterson and Wang*, 2006; *Vaniman et al.*, 2004; *Vaniman and Chipera*, 2006; *Wang et al.*, 2006, 2007, 2009]. The selected processes are as follows: the dehydration and amorphization of epsomite (7w), and the rehydration of monohydrate (LH-1w), starkeyite (4w), and amorphous Mg-sulfate (Am).

3.1. Methodology for Estimating Reaction Rates

[34] In principle, information on the reaction rates of dehydration/rehydration processes of Mg-sulfate hydrates can be extracted from the results of our experiments on stability fields and phase-transition pathways, including the 120 experiments published by *Wang et al.* [2009] at 5°C, 21°C, and 50°C, and the 30 experiments at −10°C reported in section 2 of this paper. Specifically, the data on the phase identified (by Raman spectroscopy) in the reaction products at intermediate stages and the hours (since placement of starting hydrates into RH buffers) needed for the appearance of new phases of dehydration or rehydration are critical for the rate calculation. However, our experiments were originally designed to investigate stability fields. The parameters used and the frequency of phase identification at intermediate stages of experiments were fixed. Also, because of the long duration of these experiments, repeating them is not an option. Accordingly, there are uncertainties in the rate calculations (discussed below). Thus only rough estimates of the reaction rates can be made from these data. In fact, we consider only the order of magnitude of reaction rate ratios to support the discussion in section 4.

[35] Three types of uncertainties are involved in estimating reaction rates from our experiments. First, only four temperatures (50, 21, 5, and −10°C) were chosen in our original design of stability field experiments, which limits the number of data points in the reaction rate estimation for each dehydration/rehydration process. Second, only a limited number of intermediate-stage phase identifications (Raman measurements) were made. For example, twelve Raman IDs were made during the 1979 h duration of the dehydration reaction of epsomite (the "7w→ 4w" column of Table 3) at 21°C, e.g., at 1, 7, 24, 43, 67, 134, 179, 224, 351, 686, 1143, and 1979 h since the epsomite samples were first placed in RH buffers. At 351 h (~13 days into the experiment), the total conversion of epsomite (7w) to starkeyite (4w) was observed through Raman measurements. However, the actual total conversion of 7w → 4w may have occurred at any time within the 127 h interval, between 224 and 351 h. In order to mark the time for this event (7w → 4w), we arbitrarily use the middle point of this 127 h time interval, i.e., 64 h, as the uncertainty. The third type of uncertainty comes from low T experiments (e.g., for 7w → Am process at −8°C, the "7w → Am" column of Table 3). The total conversion of 7w to the amorphous phase was not reached at 208 h; however, the experiment had to be terminated for other reasons [*Wang et al.*, 2009]. Nevertheless, gravimetric measurements were made along with the Raman characterization [*Wang et al.*, 2009, Figure 19a]. An extrapolation along the regression line of gravimetric data points was made to estimate the number of hours for total conversion (last row of the "7w → Am" column of Table 3). This estimate introduces the 3rd type of uncertainty.

[36] In Figure 8a, data for the dehydration of epsomite (7w) to starkeyite (4w) (as well as other four phase transitions in Figures 8b, 8c, 8d, and 8e) are plotted. The data symbols with full width represent the hours when Raman IDs showed that the total conversion of the starting phase was obtained. A regression line for each process was calculated using these data. The uncertainties (the 2nd and 3rd types) are plotted above the data symbols with half width in Figure 8. The five plots in Figure 8 show that compared to the long duration of the full experiments (over 3 years), the effect of a few hours or a few days on the uncertainties are quite small. Specifically, they do not affect the general trend of a regression line, i.e., these uncertainties would not affect the slopes of regression lines. Therefore, only the general trends of these regression lines are used for discussion in the following sections.

[37] The data from the experiments at −10°C are not presented in Figure 8 for the following two reasons. First, because of very slow kinetics at −10°C, and very infrequent Raman phase identifications during those experiments (Table 2, in comparison with Table 3), these data bear intrinsically larger uncertainties (2nd type). Second, no gravimetric measurements were made on the intermediate products of −10°C experiments (only Raman characterizations were conducted) because the sample vial has to be kept at T < −10°C all the time, and we are not equipped to make gravimetric measurement at this condition with acceptable accuracy. Therefore we have no basis to estimate the time duration of a total conversion for the incomplete reactions after three years in reaction (we had ten such reactions).

[38] Only limited numbers of experimental results (entries given in italic font in Table 3) were needed to extract the reaction rate for a specific process relevant to Mars. For example, the rate of dehydration of 7w → 4w was extracted from the experiments at low RH values because they

Table 3. Experimental Observations on Phase Transitions (Identified by Laser Raman Spectroscopy) of the Intermediate Reaction Products on 21 Dehydration and Rehydration Experiments[a]

7w → 4w (50°C)				LH-1w → 7w/6w (50°C)		4w → 7w/6w (50°C)				Am → 7w/6w (50°C)	
Hours	11%RH			Hours	100%RH	Hours	100%RH	74%RH	65%RH	Hours	100%RH
1	6w			1	6w, 1w	1	6w, 4w	4w, 6w	4w, 6wt	1	Am, 7w, 4w
7	4w, 6w			4	6w, 1w	*4*	*6w*	6w, 4w	4w, 6w	*4*	*6w*
24	*4w*			*23*	*6w*	*18*		*6w*	6w, 4w		
						42			*6w*		
7w → 4w (21°C)		7w → Am (21°C)		LH-1w → 7w/6w (21°C)		4w → 7w/6w (21°C)				Am → 7w/6w (21°C)	
Hours	11%RH	Hours	<0.1%RH	Hours	100%RH	Hours	100%RH	75%RH	59%RH	Hours	100%RH
1	7w, 6w	0.3	6w, Am	1	1w, 6w	1	4w,6w	4w,6w	4w	1	Am
7	6w, 7w	0.7	6w, Am	4	6w, 1w	5	6w, 4w	4w,6w	4w, 6wt	5	6w, 4w, Am
24	6w, 4wt	1	6w, Am	23	6w, 1w	*19*	*7w*	6w, 4w	4w, 6w	*21*	*7w, 6w*
43	6w	1.3	6w, Am	*44*	*6w, 7w*	*43*		*7w*	6w, 4w		
67	6w, 4w	*2*	*Am*			*68*			*6w*		
134	6w, 4w										
179	4w, 6w										
224	4w, 6wt										
351	*4w*										
7w → 4w (5°C)		7w → Am (0°C)		LH-1w → 7w/6w (5°C)		4w → 7w/6w (5°C)				Am → 7w/6w (5°C)	
Hours	11%RH	Hours	<0.1%RH	Hours	100%RH	Hours	100%RH	75%RH	59%RH	Hours	100%RH
18	7w	1	7w	1	1w, 6wt	18	4w, 6w	4w, 6w	4w, 6w	1	Am
37	7w	6	6w	4	6w, 1w	37	6w, 7w, 4w	6w, 7w, 4w	4w, 6w	31	Am, 6w
107	7w, 6w	25	6w, Am	31	6w, 1w	*107*	*7w*	7w, 4wt	6w, 7w, 4w	*190*	*7w*
207	6w, 7w	*50*	*Am*	*68*	*7w*	*207*		*7w*	7w, 4wt		
321	6w					*321*			*7w*		
631	6w										
816	6w										
7w → 4w (5°C)		7w → Am (−8°C)									
Hours	11%RH	Hours	<0.1%RH								
959	6w										
1270	6w	8	7w								
2157	6w, 4w	18.5	6w								
3044	6w, 4w	55	6w, 4w, Am								
8587	4w, 6w	157.5	6w, Am								
12802	4w, 6w	208	6w, Am								
18629	4w, 6w	*500*[b]	*Am*								
24028	*4w*										

[a]Most data are selected from *Wang et al.* [2009, Tables 2, 3, 4, 5]. One datum is from an experiment at 11% RH and 5°C that reached equilibrium only recently. The observed timings of a complete phase transition in this table (italic fonts) are used to calculate the reaction rate of a specific process at certain T-RH conditions (Figure 8).

[b]The total conversion of 7w to amorphous phase was not reached at 208 h, but the experiment had to be stopped due to other limitations [*Wang et al.*, 2009]. Using the results from gravimetric measurements (made along the Raman IDs [*Wang et al.*, 2009, Figure 19a]), an estimation on the needed hours (500) for the total 7w → Am conversion was made through an extrapolation along the regression line of these gravimetric data points.

simulate better the extremely low RH levels during the daytime on Mars. Only the results at 11% RH (the "7w→ 4w" column of Table 3, LiCl-H_2O RH buffer) were used. (The data at 6% RH (LiBr-H_2O RH buffer) were not used because amorphous Mg-sulfates appeared from the dehydration of epsomite at 6% RH). Using similar reasoning, the rates of rehydration of 1w, 4w, and Am to 7w (or 6w) were extracted from experiments at the 100% RH values (The "Am → 7w/6w," "LH-1w → 7w/6w," and "4w → 7w/6w" columns of Table 3) which correlates with the rehydration processes during the early morning hours on Mars when the relative humidity reaches 100%, as indicated by the frost observed on the Opportunity Rover [*Landis et al.*, 2007].

3.2. Reaction Rates: Estimation and Extrapolation

[39] Figure 8 demonstrates that our experimental results match very well with the Arrhenius equation:

$$\ln(k) = \ln(A) - \frac{E_a}{R}\left(\frac{1}{T}\right)$$

where k is the rate constant, A is a pre-exponential factor, E_a is activation energy, R is the gas constant, and T is absolute temperature (K). In our plots (Figure 8), the rate constant $k = 1/t$, where t is the time (in seconds) needed for a total phase conversion (e.g., 7w → 4w, Figure 8a and the "7w→ 4w" column of Table 3). A linear regression line was derived

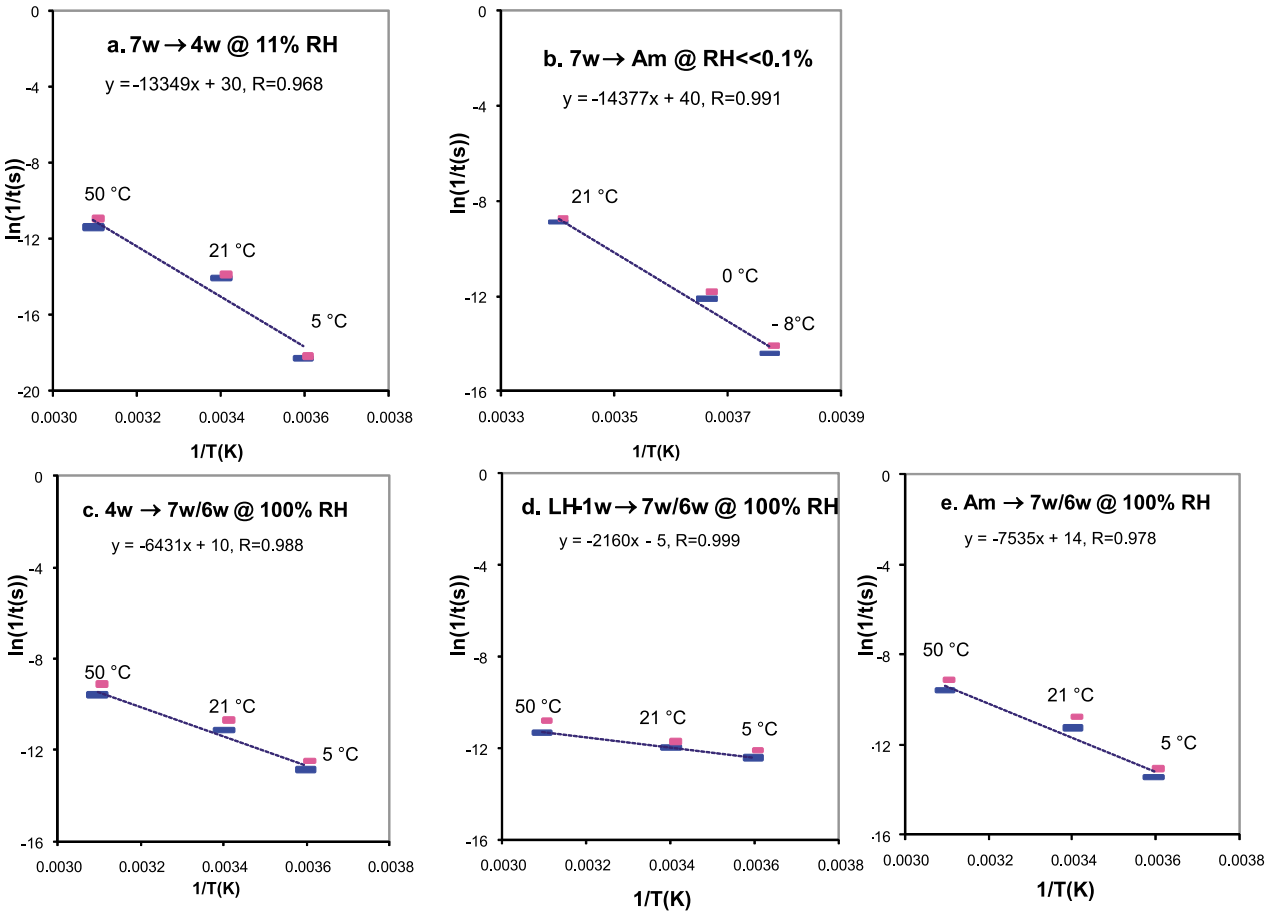

Figure 8. Temperature dependence of reaction rate for five dehydration and rehydration processes. The data symbols with full width represent the hours when Raman IDs indicated that total conversion was achieved. The uncertainties (2nd and 3rd types, see text) are plotted above the data symbols with half width. A regression line for each process was calculated from these data. The formula of the regression line and R value are as shown in each plot. The slope of regression line corresponds to the activation energy Ea of the specific process on the basis of the Arrhenius equation.

from the three experimental data sets (50°C, 21°C, 5°C) for each process (Figures 8a, 8c, 8d, and 8e; 21°C, 0°C, −8°C in Figure 8b). These regression lines have R values from 0.999 to 0.968. Note for three data points, a 90% confidence level requires an $R \geq 0.988$. Considering the three types of uncertainties discussed in section 3.1, these correlations are good enough to evaluate the reaction rates.

[40] Because all samples (except meridianiite) were prepared in the same way, the effects of grain size and sample porosity on reaction rates can be excluded. Figure 8 shows that the reaction rates of all five processes are all strongly affected by temperature, i.e., they decrease as temperature decreases. For example, the dehydration rate of 7w → 4w at 21°C and 11% RH is over 68 times faster than the rate at 5°C, but it is only 7% of the rate at 50°C (Figure 8a). The reaction rate of 7w → Am at 21°C is ~25 times the rate at 0°C and 250 times the rate at −8°C (the "7w → Am" column of Table 3 and Figure 8b).

[41] In principle, the activation energy *Ea* and pre-exponential factor (A) in the Arrhenius equation can be calculated on the basis of the regression line of each dehydration or rehydration process in Figure 8. Such a calculation for the 7w → 4w dehydration would reveal an activation energy of 1.15 eV, which is the same order of magnitude of the *Ea* (0.9 ± 0.10 eV, for epsomite dehydration) derived from a 35-step TPD (temperature programmed dehydration) experiment monitored by a quadrupole mass spectrometer in an ultrahigh vacuum chamber [*McCord et al.*, 2001]. As discussed in section 3.1, three types of uncertainties were involved in our reaction rate extraction. Among them, the type 2 uncertainty does not significantly affect the slope (related to *Ea*) of a regression line, but can affect its intercept (related to A). When considering the error propagation from the uncertainty in ln(1/t(s)) and the uncertainty for the pre-exponential factor (A), we think it is more realistic to evaluate the *ratios of Ea*(*s*). For example, for both 7w/6w ←→ 4w and 7w/6w ← → Am, the *Ea* of dehydration is about two times the *Ea* of the rehydration process, whereas the Ea(s) of 4w →7w/6w and Am → 7w/6w rehydration are about three times of the Ea for LH-1w → 7w/6w rehydration.

[42] Stated another way, the rates of two dehydration processes (7w → 4w and 7w → Am) decrease much faster with temperature than those of three rehydration processes

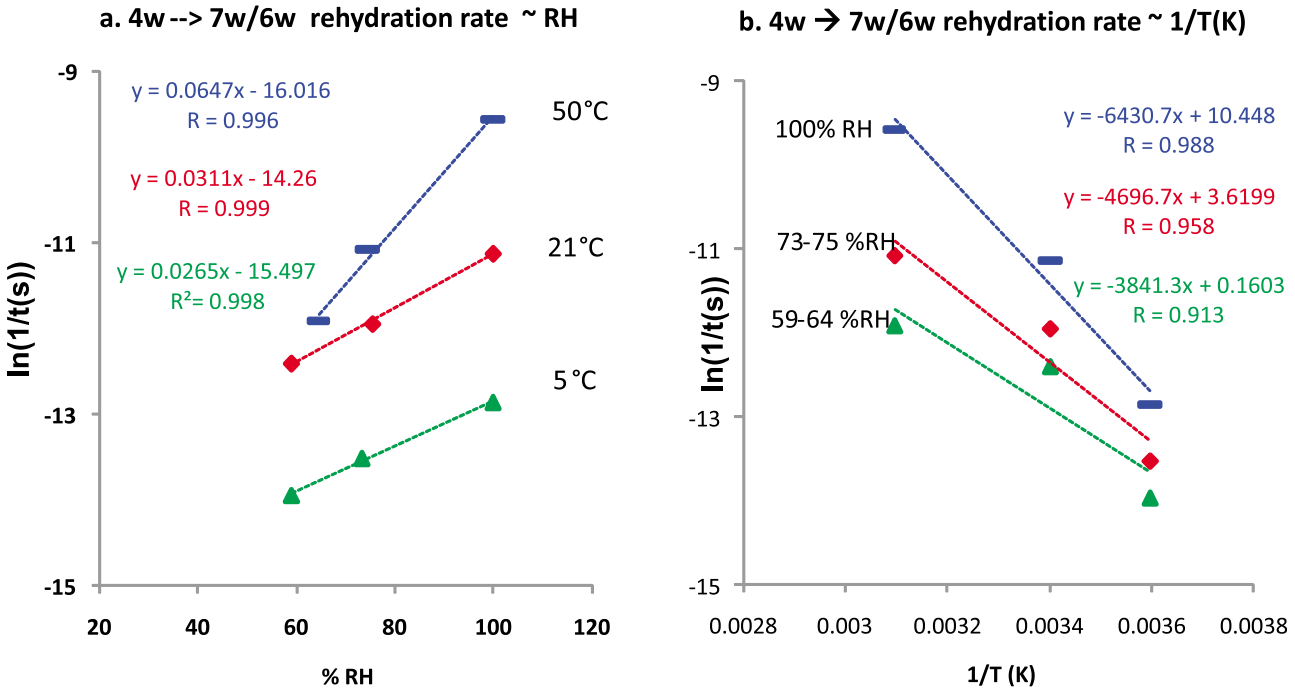

Figure 9. The (a) RH dependence and (b) temperature dependence of the rate constant for the 4w → 7w/6w rehydration process. For clarity, only the data that mark the hours when Raman IDs indicated that total conversion was achieved are presented. A regression line was calculated for each set of data: i.e., for each temperature in Figure 9a, and for each RH level in Figure 9b. The formula of the regression line and R value are as shown. For this rehydration process, the rate constant (ln(1/t)) correlates more tightly with RH (Figure 9a), demonstrated by higher correlation factor R values.

(4w, LH-1w, and Am → 7w/6w). 7w → Am has the steepest decreasing slope, and LH-1w → 7w/6w has the shallowest decreasing slope. This phenomenon can be explained by considering the two different main factors that influence the progress of dehydration and rehydration processes: temperature, and $f(H_2O)$.

[43] We infer that temperature has a greater effect on the progress of dehydration, and $f(H_2O)$ has a greater effect on the progress of rehydration, because temperature affects the thermal vibrations of atomic or ionic groups in the crystal structure, whereas $f(H_2O)$ determines the availability of H_2O molecules in the environment. For example, the 7w → Am transition occurs when structural waters are removed from epsomite rapidly, causing collapse of the epsomite crystal lattice [*Vaniman et al.*, 2004; *Wang et al.*, 2006]. The probability of a structural water molecule escaping from a crystal structure is mainly affected by its thermal vibration (i.e., temperature). At low temperature, the thermal vibrations would be damped enough to prevent the rapid escape of structural water, and the formation of crystalline starkeyite would compete with amorphization. The combination of the two effects caused the steepest decrease in slope as a function of temperature for this 7w → Am dehydration process.

[44] The reason for the reduced temperature dependence of the rate constant of the three rehydration processes (4w, LH-1w, and Am → 7w/6w) is that these processes rely more on the environmental RH, i.e., the availability of H_2O molecules. We plot the data for 4w → 7w/6w rehydration process from the "4w → 7w/6w" column of Table 3 to support this hypothesis. Figure 9a plots the rate constant ln (1/t(s)) versus RH (%) but using different symbols to mark the data obtained at different temperature (50°C, 21°C, 5°C). Figure 9b plots the rate constant ln(1/t(s)) versus 1/T (1/K) but using different symbols to mark the data obtained in a different RH range (100%, 73–75%, 59–64%). Comparing the two plots, it is obvious that the rate constant (ln(1/t)) of this rehydration process (4w → 7w/6w) correlates more tightly with RH (Figure 9a), demonstrated by a set of high correlation factor R values, 0.996, 0.999, 0.998, all of which are larger than 0.988 (the R value required by 90% confident level for three data points). In comparison, the rate constant (ln(1/t)) correlates less tightly with T (Figure 9b), demonstrated by a set of lower R values, 0.988, 0.958, and 0.913 (≤0.988).

[45] There is a general phenomenon in all three-point (ln(1/t(s) versus 1/T(K)) plots of Figures 8a–8e and Figure 9a, i.e., the linear regression lines in all plots occur below the middle data point. This feature suggests that instead of using a linear regression line, a second-order polynomial (or other type) regression line should have a better fitting for the data with improved R values (actually, a second order polynomial line yields R values from 0.999 to 1.000, better than R from 0.968 to 0.999 when using linear regression). Although we show the linear regression lines in all plots of Figure 8 for the benefit of simple and straightforward interpretation, the likely curvature of the data implies that the pre-exponential factors (A) for these processes may have a weak temperature dependence, further indicating that these dehydration/rehydration processes probably have higher than zero-order kinetics.

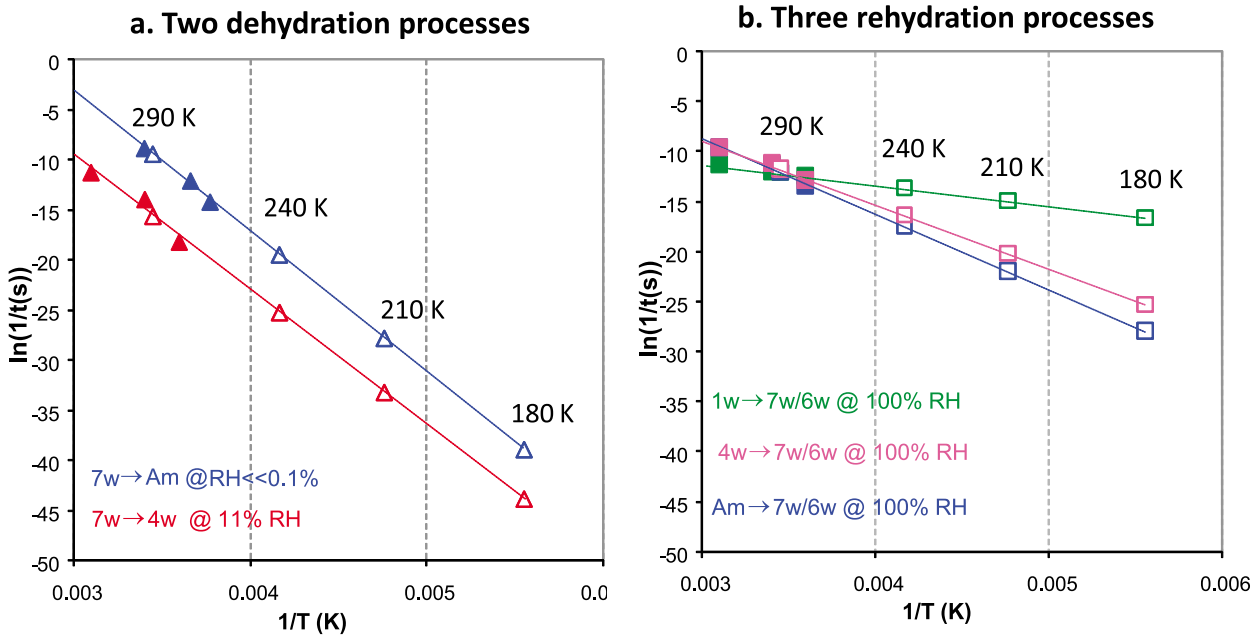

Figure 10. A rough estimate of the relative rates of five dehydration/rehydration processes at low temperatures relevant to Mars can be made through extrapolation, using the experimentally derived pre-exponential factor(s) A and activation energy(s) E_a. The extrapolated data points are shown as open symbols.

[46] Zero-order kinetics would normally be used to describe sublimation of water ice, as a homogenous bulk material. On the other hand, the rate of dehydration/rehydration processes for a hydrous sulfate should be limited by the diffusion rate of H_2O molecules within the sample. During the dehydration of an epsomite grain ($MgSO_4{\cdot}7H_2O$), the structural H_2O molecules diffused from the grain core could be captured multiple times by vacancy sites (and weak potential energy fields) en-route to the grain surface; such vacancy sites would be left by H_2O molecules that escaped from the grain early in the dehydration process. Therefore, higher than zero-order kinetics should be used to describe the dehydration of hydrous salts, such as those experimentally determined by *McCord et al.* [2001] for epsomite, mirabilite ($Na_2SO_4{\cdot}10H_2O$), and natron ($Na_2CO_3{\cdot}10H_2O$). Although we do not have enough experimental data points to fit a first-order Arrhenius equation, our observations (Figures 8a–8e and Figure 9a) suggest that all five dehydration and rehydration processes behave similarly, i.e., they have higher than zero-order kinetics. The implication of this conclusion is that the hydrous Mg-sulfates have greater thermal stability than that of water ice.

[47] Our thirty experiments at −10°C have lasted for more than three years, yet only 2/3 of them (RH < 22%) have reached equilibrium. Because of the extremely slow reaction rates, we do not plan to conduct systematic experiments at even lower temperatures as observed on Mars (~180 K) [*Smith et al.*, 2004, 2006; *Spanovich et al.*, 2006]. Nevertheless, we can reach a rough estimate of the relative rates of five dehydration/rehydration processes at temperatures relevant to Mars surface and subsurface through extrapolation, using the experimentally derived pre-exponential factor(s) A and activation energy(s) E_a. The extrapolated data points are shown in Figure 10 as open symbols.

[48] Each of the regression lines shown in Figures 8 and 10 represent the temperature dependence of the reaction rate for a specific dehydration or rehydration process. As discussed in section 3.1, because the uncertainties involved in estimating reaction rates do not affect the general trend (i.e., the slope) of a regression line, the rate ratios at different temperatures are scientifically meaningful. Moreover, considering the differences in our experimental setting from the real conditions on Mars (surface and subsurface) and the uncertainties associated with extrapolation, only the orders of magnitude of the rate ratios will be considered in the discussion of section 4. Table 4 lists the rate ratios in the form of the order of magnitude, for two important dehydration reactions (7w → 4w and 7w → Am, Figure 10a) and three rehydration reactions (LH-1w → 7w/6w, 4w → 7w/6w, and Am → crystalline 7w/6w, Figure 10b), compared to the same type of reactions at 294 K in laboratory (21°C, the "Duration" and "Rate" columns of Table 4).

[49] On the basis of data in Table 4, we can say that the dehydration of epsomite (7w) would move forward fast during daytime but would slow down considerably when temperature drops to ~240 K (−33°C) as it does during the early evening hours on Mars in equatorial regions, because the dehydration rate would only be 10^{-5} times (the "240 K" column of Table 4) the rate at 294 K (21°C) (the "Rate" column of Table 4). This rate corresponds to a 2984 year duration to make the 7w → 4w transition, which occurs in 351 h at 21°C and 11% RH in our laboratory setting. Similarly, when the temperature drops to ~180 K (−93°C) during the early morning hours on Mars in equatorial regions, the rehydration rates of LH-1w, 4w, and Am would be 10^{-3} to 10^{-8} times (the "180 K" column of Table 4) the

Table 4. Reaction Rate Ratios (Order of Magnitude) of Five Dehydration and Rehydration Processes of Mg-Sulfates Important for Mars Sulfate Mineralogy[a]

			Daytime on Mars		Nighttime on Mars	
Temperature			290	240	210	180
Duration in hours at Gusev [*Smith et al.*, 2004, 2006]			>10	1–2	1–2	1–2
Estimated RH values based on the work of *Smith* [2002]			~0%	<1%	1–10%	~100%
	Duration (hours) at 294 K	Rate (1/s) at 294 K	Rate Ratios Against the Rates at 294 K			
			290 K	240 K	210 K	180 K
Dehydrations						
7w → 4w at 11% RH	351	8E-07	*4E-01*	*1E-05*	*5E-09*	1E-13
7w → Am at <0.1% RH	2	1E-04	6.E-01	*3E-05*	*6E-09*	9E-14
Rehydrations						
4w → 6w/7w at 100% RH	19	1E-05	7E-01	5E-03	*1E-04*	*7E-07*
1w → 6w/7w at 100% RH	44	6E-06	1E+00	2E-01	*5E-02*	*9E-03*
Am → crystalline at 100% RH	21	1E-05	1E+00	2E-03	*2E-05*	*6E-08*

[a]Data in four columns at the right side of this table are rate ratios at four Mars relevant temperatures against the rates at 294 K (21°C). These ratios were obtained through the extrapolations of rate constant vs. T correlation shown in Figure 10. Italic font marks the rate ratios during a period when the specific dehydration or rehydration process would be favored at the RH conditions on Mars, indicated in Figure 11 as periods 1, 2, and 3.

rates at 294 K (21°C) for the rehydration of Am and 4w (the "Rate" column of Table 4).

4. Implications for the Phase Stability and Phase Transitions of Mg-Sulfates on Mars

[50] The results from our experimental studies and those of others on the phase boundaries, stability and metastability fields, phase transition pathways, and reaction-rate ratios (order of magnitude only) of Mg-sulfate hydrates can be used to determine the most common Mg-sulfate species that should be present at or near the Martian surface in different time periods and locations.

4.1. T and RH Conditions on Mars

[51] To determine what phases should be stable at the surface (exposed to atmosphere), we need to know the actual water-vapor pressure and Martian surface temperature variations during diurnal and seasonal changes. The Martian surface temperature range observed during the Viking primary mission was 130–290 K [*Kieffer et al.*, 1977]. The near-ground air temperature measured by Mars Pathfinder during the diurnal cycle was about 265–195 K [*Schofield et al.*, 1997]. The best and longest-term surface-temperature measurement has been made by the two Mars Exploration Rovers during their 7+ years of exploration at two near-equatorial sites. Ground temperature data have been derived from MiniTES observations and show a repeatable pattern for each Martian year [*Smith et al.*, 2004, 2006; *Spanovich et al.*, 2006]. The temperature extremes observed in the first two years at Gusev are about ~290 K and ~180 K. The magnitude of temperature changes in the diurnal cycle vary according to seasons on Mars.

[52] The observation using TES (Thermal Emission Spectrometer) on Mars Global Surveyor has provided information on seasonally averaged water-vapor pressures on Mars [*Smith*, 2002]. About 16 precipitation-μm or 16×10^{-3} kg/m^2, 0.16 Pa $f(H_2O)$ was derived for the zone including Gusev, and 14 precipitation-μm or 14×10^{-3} kg/m^2, 0.14 Pa $f(H_2O)$ for the zone including Meridiani Planum. Combining the measured temperatures [*Spanovich et al.*, 2006, Figures 2 and 3] and the seasonal average $f(H_2O)$ data, we have produced a rough plot of RH variation during the diurnal cycle for different seasons at the Spirit site in Gusev Crater (Figure 11; M. Wolff, unpublished MiniTES-derived temperature data, 2006).

[53] Figure 11 demonstrates three characteristics of RH variations during three periods at the surface of the Spirit site: (1) during daytime (~08:00–18:00 local solar time on Mars), the RH level at the surface (for all seasons) is ~0.01–0.1% within a temperature range of 290–240 K; (2) during early morning periods (~0:00–04:00 local solar time on Mars), the RH level can reach 100% and can start to form frost (frost was observed on the Opportunity rover body at the Meridiani Planum site [*Landis et al.*, 2007]). This period only lasts 2–4 h depending on the season; (3) between these two periods, i.e., ~04:00–08:00 local solar time on Mars, the RH level would experience a rapid drop, from 100 to 10% RH (~207 K) in 2–3 h, and then to <1–0.1% RH (~224 K) in 4–5 h, depending on the season.

[54] The long daytime hours with extreme low RH provide the main conditions for dehydration of Mg-sulfates; the short hours in early morning period with high RH would facilitate rehydration, whereas the period with rapid RH decrease would favor amorphization [*Vaniman et al.*, 2004; *Wang et al.*, 2006, 2007]. However, whether a process can actually progress and produce detectable secondary phases depends on the rate of that particular process within the temperature ranges corresponding to those three periods (Table 4), and the duration of these temperature ranges at the surface of Mars (Figure 11 and Table 4).

[55] To evaluate the likelihood of certain processes occurring on Mars in the following section, we combine current knowledge of (1) Martian surface T and RH variation (Figure 11 for equatorial regions) [*Smith et al.*, 2004, 2006; *Spanovich et al.*, 2006], (2) results from ours and others' experiments on the stability fields and phase-transition pathways of Mg-sulfates [*Chou and Seal*, 2003, 2007; *Chipera and Vaniman*, 2007; *Peterson and Wang*, 2006; *Vaniman et al.*, 2004; *Vaniman and Chipera*, 2006; *Wang et al.*, 2006, 2007, 2009], and (3) the rate ratios (order of

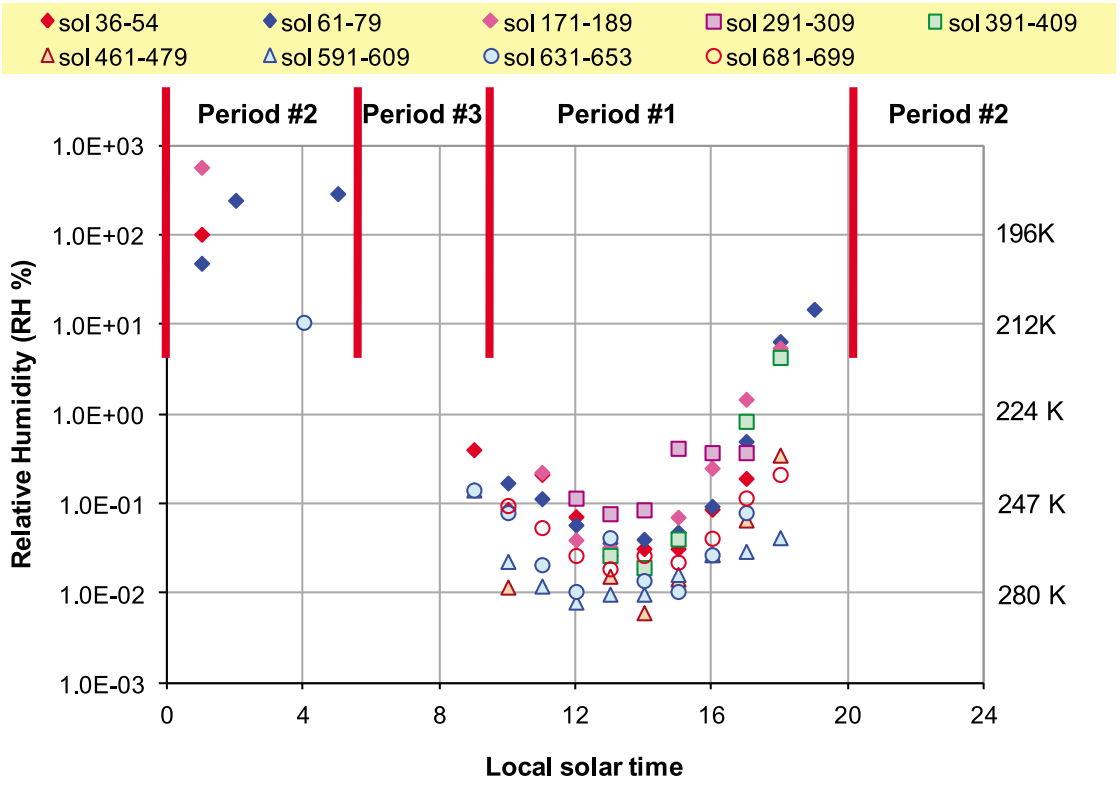

Figure 11. RH variations during the diurnal cycle at Gusev Crater on Mars. The corresponding temperatures are marked on the right side of the plot. The surface temperature was derived from MiniTES observations by Spirit at Gusev Crater (M. Wolff, unpublished MiniTES-derived temperature data, 2006). The RH values were calculated from these temperatures and the seasonal average $f(H_2O)$ data derived from TES (Mars Global Surveyor) observations in the Gusev region [*Smith*, 2002]. The vapor pressure of liquid water [*Haar et al.*, 1984] for T > 273 K and vapor pressure of ice [*Mason*, 1971] for T < 273 K were used in calculations. Four red vertical lines separate the three time zones during a Martian sol, as discussion in the text (see section 4.1).

magnitude only) at different temperatures estimated in this study for five phase-transition processes of Mg-sulfates (Table 4). From this evaluation and the experimental observations, we infer the species of Mg-sulfates that should be stable on Mars at different periods and locations.

4.2. Precipitation of Mg-Sulfates From Aqueous Solutions

[56] Because the surface temperatures on Mars were never much greater than 323 K (50°C), even during its potentially warm and wet past, phase boundary studies [*Chou and Seal*, 2003, 2007] suggest that epsomite (7w), not hexahydrite (6w), would be the major Mg-sulfate phase precipitated from Mg- and S-bearing aqueous solutions (except in polar regions) (shown in Figure 12). Meridianiite (11w) would precipitate from low temperature Mg- and S-bearing aqueous solutions at locations where T < 275 K (2°C) (shown in Figure 12) (based on the work of *Peterson and Wang* [2006] and this study). When the temperature of an Mg- and S-bearing aqueous solution exceeded 342 K (69°C), i.e., during a localized hydrothermal event, kieserite (MH-1w) would be the precipitation product (shown in Figure 12) (based on the works of *Chou and Seal* [2007] and *Wang et al.* [2009]).

4.3. Dehydration of Mg-Sulfates

[57] As regions of the Martian surface have become colder and drier over geologic time, the most hydrous Mg-sulfates, epsomite (7w) and meridianiite (11w), exposed near the surface would be expected to dehydrate. Below 273 K (0°C), as coexisting H_2O-ice disappears, meridianiite (11w) would convert readily to a heptahydrate Mg-sulfate (LT-7w, Figure 12), which has, as demonstrated in section 2.2, a slightly distorted structure from epsomite. In low temperature regions (poles and subsurface), the RH range for the stable existence of LT-7w is very large (Figure 1). The rehydration of Am to LT-7w in LiBr and LiCl RH buffer solutions at −10°C (Figures 1 and 7) demonstrated a low RH limit of ~13% for the LT-7w stability field, which is significantly lower than the RH limit of ~34% at 5°C for epsomite (7w). At T > 273 K (0°C), the LT-7w phase would first convert to normal epsomite (RT-7w), and then dehydrate.

[58] The Martian subsurface, however, can have very different environmental conditions than those at the surface, as evidenced by spectral changes of ferric sulfates in salty soils excavated by Spirit after 175 sols of exposure [*Wang et al.*, 2008; *Wang and Ling*, 2011]. In the subsurface, large quantities of ice or hydrous sulfates buried together would

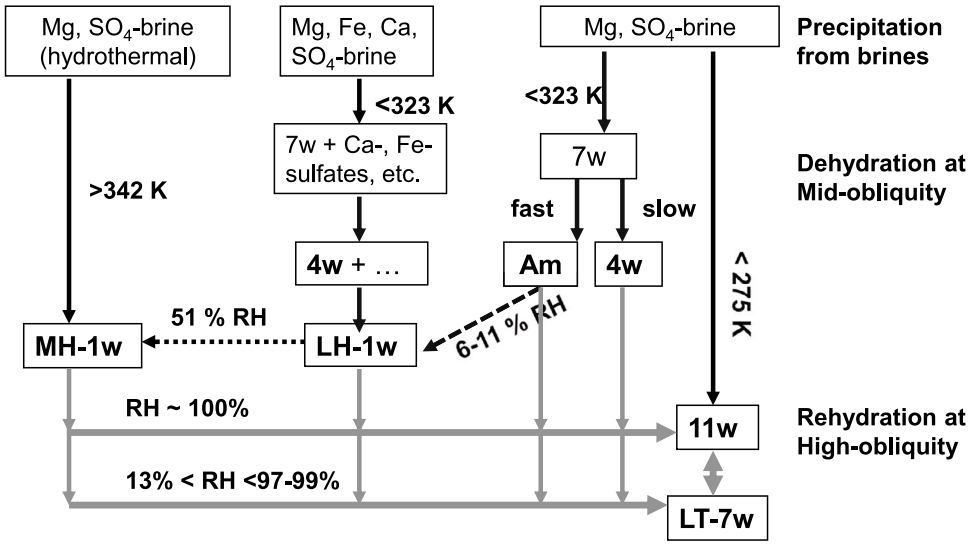

Figure 12. Precipitation and phase transitions of Mg-sulfates on Mars. Black arrows indicate precipitations and dehydrations [*Wang et al.*, 2009]. Gray arrows indicate rehydration paths (this study).

form a natural buffer to maintain a locally high $f(H_2O)$. Additionally, differences in the thermal inertia of surface regolith and subsurface sulfate- and ice-rich soils may help to sustain a sharp temperature gradient, which would yield a much lower average temperature and smaller temperature range that is less affected by the diurnal temperature cycle at the surface [*Mellon et al.*, 2004]. These conditions would facilitate the persistence of LT-7w Mg-sulfate.

[59] At temperatures between 224 and 290 K (i.e., during daytime in equatorial to midlatitude regions, period 1 in Figure 11, >10 h duration per sol), the rate of epsomite dehydration (Table 4) indicates that this process can progress, even though it will be slowed in the evening hours (Table 4). Thus over geological time, the dehydration of epsomite at the surface would progress such that all epsomite at the surface would be dehydrated.

[60] The normal product from the dehydration of epsomite on Mars should be starkeyite (4w, Figure 12). The energy barrier imposed by Martian surface temperatures (past and present) would prevent direct dehydration from epsomite (7w) to monohydrate (LH-1w). Moreover, starkeyite has a broad stability/metastability field (Figure 1) in mid-low temperature conditions and low relative humidity (−10 to 50°C and 6 to 34% RH in our experiments) [*Chou and Seal*, 2007; *Chipera and Vaniman*, 2007; *Wang et al.*, 2009]. Starkeyite has a similar NIR spectral pattern to that of polyhydrated sulfate, found on Mars with wide distribution.

[61] The dehydration of epsomite (7w) can progress to reach the monohydrate stage (LH-1w) on Mars under two circumstances (Figure 12), as follows: (1) The LH-1w could form at locations where the chemistry of original brine allowed the coprecipitation of Ca-sulfates and Fe-sulfates or allowed the coexistence of Mg-sulfates with other minerals (including Fe-oxides). Our experiments [*Wang et al.*, 2009] suggest that some coexisting species would function as a catalyst in the dehydration process of epsomite to help overcome the kinetic barrier and to reach the monohydrate stage (LH-1w in Figure 12); (2) At locations where amorphous Mg-sulfates first formed by rapid dehydration of epsomite, a continuous reduction of $f(H_2O)$ could further drive the dehydration of the amorphous Mg-sulfate phase (with irregular and less-stable structure) to the monohydrate stage (LH-1w in Figure 12) [*Wang et al.*, 2006, 2009]. We note that the monohydrate Mg-sulfate (LH-1w) formed as the end product of these two dehydration processes has a structure different from that of kieserite (MH-1w). In addition, LH-1w phase is very stable in the T-RH range relevant to Martian surface conditions [*Chipera and Vaniman*, 2007; *Wang et al.*, 2009]. LH-1w can convert to the kieserite structure (MH-1w), but only under a higher RH level and at moderate temperature (at 51% RH and 50°C in experiments reported by *Wang et al.* [2009], shown as dotted line in Figure 12). In other words, the likelihood of LH-1w to MH-1w conversion is very low under current Martian surface conditions.

[62] Based on our observations, LH-1w would be more common than MH-1w (kieserite) on the Martian surface because it is the direct dehydration product from epsomite (7w), hexahydrate (6w), and starkeyite (4w) and is very stable under conditions relevant to the surface of Mars (P, T, RH) [*Chipera and Vaniman*, 2007; *Wang et al.*, 2009]. MH-1w (kieserite) could precipitate from high-temperature Mg-S-bearing brine, thus it could occur in localized areas where hydrothermal events had occurred. Although NIR spectra of kieserite have been observed by Mars orbital remote sensing [*Arvidson et al.*, 2005; *Gendrin et al.*, 2005] in large areas, these spectra would probably be contributed mostly by LH-1w because of the low S/N of remote sensing data and the minor spectral differences of LH-1w and MH-1w (section 2.2.2).

4.4. Rehydration and Dehydration of Mg-Sulfates in the Diurnal Cycle

[63] During a diurnal cycle on present-day Mars (moderate obliquity) at equatorial region, the surface temperature fluctuation can be over 100 K. The extremely low temperature (~180 K) during the early morning hours brings the relative humidity up to 100%, demonstrated by frost

observed on Opportunity rover body [*Landis et al.*, 2007]. However, this high RH period (period 2 in Figure 11) lasts only a few hours in the early morning (i.e., 1–2 h at 100% RH, Figure 11), and more importantly, the temperature is extremely low in that period (~180–210 K). On the basis of the extrapolated rate ratios in Table 4, the rates of rehydration of LH-1w and 4w in this temperature range are thousands to tens of millions times lower than those at 294 K (21°C) (when, in our experiments, 19–44 h were needed to complete the rehydration). Moreover, on the Martian surface, this time window (1–2 h) is immediately followed by over 12 h of conditions favorable to dehydration at RH < 1% (Figure 11) with a much higher reaction rate (224–290 K). Therefore, it is unlikely that these rehydration processes would proceed and generate detectable rehydration products (7w) on the Martian surface during the diurnal cycle at moderate obliquity.

[64] Similarly, the likelihood of forming amorphous Mg-sulfates during a diurnal cycle at moderate obliquity is also very low based on the rate ratios shown in Table 4. The critical condition to form amorphous Mg-sulfates is to rapidly extract H_2O from Mg-sulfates with high degrees of hydration (i.e., epsomite, hexahydrite, and meridianiite, but not starkeyite [*Wang et al.*, 2006]), thus causing collapse of their structures. The best time window on the Martian surface to form amorphous Mg-sulfates would be during the rapid drop of relative humidity from 100 to 10% at about 180 to 207 K and from 10 to <1% at 207 to 224 K (period 3 in Figure 11). However, our vacuum desiccation experiment at −8°C (265 K) demonstrated [*Wang et al.*, 2009]: (1) the reaction rate was extremely low; and (2) two competitive dehydration processes. i.e., 7w → 4w and 7w → Am, occurred at such low temperature. We found that starkeyite (4w) started to form between 19 to 55 h vacuum desiccation at −8°C, then amorphization occurred after 158 h, and continued until the end of this experiment (208 h). At −8°C (265 K), it appears that the two competitive dehydration processes start to occur, but eventually amorphization wins the competition. At temperatures much lower than 265 K (period 3 in Figure 11), we anticipate the rate of amorphization becoming so low that the 7w → 4w dehydration process may take over. On the basis of this observation, as well as the low rate of amorphization at low temperature and the low rate of epsomite formation (from rehydration of LH-1w and 4w) as the starting phase for amorphization (Table 4), we conclude that the amorphous Mg-sulfates could not be a common Mg-sulfate phase at the Martian surface. Our conclusion contradicts that of *Vaniman et al.* [2004], who suggested amorphous Mg-sulfates can be a common phase due to the rapid dehydration in the diurnal cycle (i.e., RH change) in moderate obliquity periods, but the reaction rate was not considered in their discussion.

4.5. Rehydration of Mg-Sulfates During Periods of High Obliquity

[65] During periods of high obliquity, H_2O-ice would form at low latitudes [*Head et al.*, 2005, and references therein]. At locations where Mg-sulfates exist, coexisting H_2O-ice should stimulate the rehydration of the monohydrate (LH-1w and MH-1w) and starkeyite (4w). The temperature effect of an "ice age" in Mars' equatorial regions (M. Mellon, personal communication, 2011) would be to have cold temperatures in the daytime but comparatively mild temperature in the nighttime, i.e., smaller temperature fluctuation during the diurnal cycle compared with that at moderate obliquity (present-day Mars). Compared with the rehydration rate during the early morning hours of Mars today (moderate obliquity, i.e., Table 4), the rehydration of monohydrate Mg-sulfates (MH-1w and LH-1w) and starkeyite (4w) would proceed at a higher rate in the high obliquity period. More importantly, this rehydration would proceed more or less continuously during daytime and nighttime in coexistence with H_2O-ice (i.e., at 100% RH). Because high obliquity periods on Mars can last for tens of thousands of years, these rehydration processes can progress to completion. LT-7w and meridianiite (11w) [*Peterson and Wang*, 2006] would be the rehydration products. Depending on the actual temperature at various locations and the stability of ice, LT-7w ←→ 11w transitions could occur.

5. Conclusions

[66] Combining all of the above inferences, we conclude that in periods of moderate obliquity such as currently on Mars, LH-1w and 4w (both formed from the dehydration of epsomite and meridianiite) should be the most common Mg-sulfates seen at the surface, whereas MH-1w as a precipitation product from hydrothermal aqueous solutions could also exist locally. In polar regions or within the subsurface where the temperature is <273 K, meridianiite and LT-7w would be the most stable Mg-sulfates. Between the two, meridianiite is stable in a narrow high RH range, mostly coexisting with H_2O-ice; LT-7w is stable over a very wide RH range (~13% RH was the lower limit in our experiments at −10°C). During periods of high obliquity, MH-1w, LH-1w, and 4w should all rehydrate, with LT-7w and 11w as the rehydration products.

[67] Our study on reaction rates of five dehydration/rehydration processes of Mg-sulfates raised the importance of kinetics, on the basis of current Martian surface environmental conditions (low $f(H_2O)$, low temperature, and large changes in temperature). The slow reaction rates of many processes at low temperature affects the actual existence of hydrous sulfates on Mars, even they are permitted by thermodynamics. The slow kinetics also means that knowledge on the phase transition pathways and the persistence of metastable phases are very important.

[68] Another major result from the reaction rate extraction is that all five dehydration and rehydration processes of Mg-sulfates match Arrhenius equation but have higher than zero-order kinetics. This observation implies that hydrous Mg-sulfates have higher thermal stability compared to that of water ice (that has zero-order kinetics). During these processes, the structural water molecules diffuse through the crystal structure by overcoming a local potential energy field in crystal lattice. Therefore, the dehydration of Mg-sulfates would be slower than the sublimation of water ice in period of low obliquity, and the rehydration of Mg-sulfates would be slower than the formation of water ice in period of high obliquity. This inference is supported by observations of enrichment of "water-equivalent-hydrogen" by the Neutron Spectrometer on Odyssey over two large equatorial regions on Mars down to <1 m depth, where ground ice would not

be stable and where both the Spirit and Opportunity rovers have found hydrous sulfates in subsurface regolith.

Appendix A: Samples and Experiments

A1. Preparation of Starting Mg-Sulfate Hydrates

[69] Five hydrated Mg-sulfates were used as the starting phase for thirty experiments at −10°C and six different relative humidity levels. They are monohydrate $MgSO_4{\cdot}H_2O$ (LH-1w), amorphous $MgSO_4{\cdot}2H_2O$ (Am), starkeyite ($MgSO_4{\cdot}4H_2O$; 4w), epsomite ($MgSO_4{\cdot}7H_2O$; 7w), and meridianiite ($MgSO_4{\cdot}11H_2O$; 11w).

[70] Compounds $MgSO_4{\cdot}H_2O$ (Sigma-Aldrich, >97%, Batch 12426BC) and $MgSO_4{\cdot}7H_2O$ (Sigma-Aldrich, >98%, Batch 084K01061) were used to prepare the starting Mg-sulfate hydrates. $MgSO_4{\cdot}7H_2O$ (7w) was stored at room temperature (21°C) over a 75% relative humidity (RH) buffer for a few days to convert trace amounts of hexahydrite ($MgSO_4{\cdot}6H_2O$; 6w) to 7w. Starkeyite (4w) was produced from $MgSO_4{\cdot}7H_2O$ (7w) at room temperature over a 35% RH buffer [*Wang et al.*, 2009]. Amorphous $MgSO_4{\cdot}2H_2O$ (Am) was prepared from $MgSO_4{\cdot}7H_2O$ (7w) by vacuum desiccation (100 mτ) at room temperature [*Wang et al.*, 2006]. Compound $MgSO_4{\cdot}H_2O$ (Sigma-Aldrich, >97%, Batch 12426BC) was used directly, whose XRD, Raman, and IR spectra suggest a slightly different structural form (LH-1w) than that of kieserite (MH-1w). LH-1w is a very important dehydration product for Mg-sulfate hydrates with its own specific stability field (details of structures, spectra, and formation conditions were described by *Wang et al.* [2009]). Meridianiite (11w) was prepared by dissolving $MgSO_4$ in water (with >14 molar ratio of H_2O:$MgSO_4$) in an open dish, which was placed in a sealed container over crushed H_2O-ice and maintained at −10°C for several days. Identification of the sample as meridianiite (11w) was made through its low-temperature powder X-ray diffraction pattern, Raman spectroscopy, and measurements of mass loss on heating in air at 400°C. The homogeneity of each starting hydrate was confirmed by 30–50 spot laser-Raman analyses.

[71] With the exception of meridianiite (11w) that cannot be easily handled at room temperature, starting sulfates were ground and sieved to less than 75 μm. For each of thirty experiments, about ~0.2 g of starting Mg-sulfate was spread over the bottom of a 20 ml Kimax® pyrex scintillation reaction vial.

A2. RH Values of Binary Salt-H_2O Humidity Buffers at −10°C

[72] The humidity buffer technique [*Greenspan*, 1977; *Chou et al.*, 2002] was used to induce the phase transitions at −10°C. Each reaction vial (without cap) was placed upright in a 60 mm diameter, straight-wall glass bottle (tightly capped) that contained the saturated binary aqueous solution of a salt as a RH buffer. Six salts (LiBr, LiCl, $MgCl_2$, KI, NaCl, and KCl) were selected to provide RH buffer solutions for these low-T experiments; all of these have eutectic temperatures below −10°C (the highest is −11.8°C for KCl aqueous solution), such that these buffer solutions did not freeze at the selected T (−10°C) of experiments. Each RH buffer jar that contains a sample vial was partially submersed in a bed of silica sand (as a thermal contact medium), and stored in a freezer at a temperature of −10°C ± 2°C for 43–46 months.

[73] We are unaware of RH values of saturated binary aqueous solutions of salts at temperatures below 0°C, thus we used two methods to estimate the RH values (or ranges) of the six selected RH buffers. All of these methods, however, contain associated uncertainties.

[74] The first method is to convert *Greenspan*'s [1977] RH values of buffer solution (x) to water vapor pressures $f(H_2O)_x$, and then to find a correlation between $f(H_2O)_x$ and temperature (T) for each saturated aqueous solution of binary salt (x) above 0°C (limit of T in the work of *Greenspan* [1977]). This correlation can then be extrapolated to −10°C to find the $f(H_2O)_x$ values. The ratio of the $f(H_2O)_x$ over the vapor pressure of water-ice at −10°C was finally taken as the RH value of that buffer solution (x) at −10°C (Table 1). The major source of error in this procedure is from the extrapolation to −10°C, especially when there is a phase transition in salt in this temperature range (e.g., NaCl to NaCl.$2H_2O$ transition at 0.1°C). In addition, although a sixth-order polynomial regression was used to find the $f(H_2O)_x$ versus T correlations, some correlation curves (e.g., LiBr and NaCl) show irregular changes in the slopes when extrapolating to −10°C, which affects the estimated $f(H_2O)_x$ values as well as RH values. RH values that may have large errors are not listed in Table 1, with the corresponding cell marked with an asterisk.

[75] The second method is by directly measuring the relative humidity in a sealed bottle that contains an RH buffer solution using a Traceable® Hum./Temp/Dew Point meter (No. 4085 from Control Company). The bottle containing RH buffer solution was placed inside the freezer (maintained at −10°C ± 2°C), with the RH probe inserted (through the seal) in it. For each buffer solution, 10 to 15 measurements were taken over the course of two days. Because of the temperature fluctuation of the freezer (−10°C ± 2°C), the measured RH values vary in a range for each RH buffer solution. These ranges are listed in Table 1, compared with the extrapolated RH values. The measured RH ranges are used in the description of our experimental results in section 2. Although less accurate than desired, these RH ranges are sufficient to separate the zones of RH for understanding the stability field and phase transition pathways of Mg-sulfates at low temperature.

A3. Phase Identifications at Low Temperature

[76] The phase identification (ID) of the intermediate products (done at regular time interval for each of thirty experiments through 43–46 months experimental duration) from dehydration or rehydration processes was done by direct laser Raman spectroscopy at the temperature of dry ice (−78.5°C). A Kaiser Holoprobe RXN Raman system (532 nm excitation wavelength), fitted with a fiber-optic-coupled probe, was used. For this operation, the sample vials were quickly removed from the RH buffer bottles (at −10°C ± 2°C), quickly capped, and stored on a bed of dry ice within a foam box. A curtain made of thin plastic film isolates the space between the Raman probe (with a 2.5″ focal length) to the foam box from the surrounding laboratory air. During a Raman measurement, the sample vial,

resting on a bed of dry ice, was uncapped and the laser beam focused on the sample powder surface through the open top of the vial. The cold CO_2 gas sublimated from dry ice filled the space surrounded by the plastic film curtain and protected the sample from direct contact with laboratory air. For each sample of an intermediate stage, three Raman measurements (<3 min) on three spots were taken. The identified phases from all three Raman spectra are listed in Table 2. After the measurements, the vial was recapped and temporarily stored in the foam box with dry ice until its return to the RH buffer bottles in the freezer. Because of the low temperature (−78.5°C) and the sample isolations during short Raman measurements, the probability of phase transition was extremely low. Different from the experiments at 5°C, 21°C, and 50°C reported earlier [*Wang et al.*, 2009], gravimetric measurements cannot realistically be made for the intermediate products of these 30 experiments at −10°C.

[77] The diffuse-reflectance VIS-NIR spectra (0.35 to 2.5 μm) of prepared meridianiite and LT-7w heptahydrate samples were collected using an Analytical Spectral Device (ASD) spectrometer at dry ice temperature. The metal holder used for the ASD powder sample measurement was first brought into thermal equilibrium with a bed of dry ice in a foam box, and then the sample powder (stored in the same foam box with dry ice) was spread into the cold holder. The cold CO_2 gas sublimated from dry ice protected the sample from direct contact with laboratory air, and the VIS-NIR measurement was immediately made with a duration of <30 s. The sample was discarded after each diffuse reflectance measurement. Repeated measurements (when necessary) were always made on fresh sample powder.

[78] X-ray diffraction measurements were made using a Rigaku Geigerflex X-ray diffractometer with Cu Kα radiation. We used a customized XRD sample mount to measure the diffraction patterns of meridianiite and LT-7w samples kept at dry-ice temperature (−78.5°C). The XRD sample mount is attached to a small dry-ice box, both are made of aluminum. When the box is filled with dry ice and attached to the sample mount, but not inserted into the X-ray diffractometer, the sample can be kept at −78.5°C for ~24 min. In order keep the sample at dry-ice temperature for long-duration measurements within X-ray diffractometer, we added a flow of cool N_2 gas (at about 180 K, released from liquid N_2 by heating resisters in an LN_2 Dewar) through the sample chamber of our X-ray diffractometer. This setup allowed us to keep the entire sample mount at dry-ice temperature for >15 min, long enough to acquire an X-ray diffraction pattern with small scan step (0.04°) and acceptable S/N (dwell time 1 s). The sample was discarded after each XRD measurement.

[79] In order to verify the amount of structural water in prepared meridianiite and in LT-7w and RT-7w heptahydrate, the samples were placed in ceramic cups and baked at 400°C in an Isotemp^R muffle furnace (Fisher Scientific) for three days. Anhydrous $MgSO_4$, identified by Raman measurements, was the final phase of all three samples. Gravimetric measurements (using a PM480 DeltaRange electronic balance from Mettler-Toledo, Inc., with a precision ±1 mg for repeat measurements) were conducted on all three samples before and after baking. These measurements confirmed that eleven water molecules per SO_4 were lost after 400°C baking for the prepared meridianiite sample, and seven water molecules per SO_4 were lost for the prepared LT-7w and RT-7w samples.

[80] **Acknowledgments.** This work was supported by NASA grants NNG05GM95G, NNX07AQ34G, NNX10AM89G, and NASA contract 1295053. We are thankful for R. Peterson in conducting the low temperature XRD pattern calculation of $MgSO_4 \cdot 7D_2O$, for M. Mellon in communicating his insight of Martian temperature variations, for M. Wolff in providing the surface temperature data measured at the Spirit site, and for Y. L. Lu in helping some the laboratory measurements. Furthermore, we would express our appreciations to M. Zolotov and V. Chevrier, for their critiques and suggestions that helped improve this manuscript. The use of trade product, industry, or firm names in this report is for descriptive purposes only and does not constitute endorsement by Washington University or the U.S. Government.

References

Ackermann, S., B. Lazic, T. Armbruster, S. Doyle, K. D. Grevel, and J. Majzlan (2009), Thermodynamic and crystallographic properties of kornelite [$Fe_2(SO_4)_3 \cdot 7.75H_2O$] and paracoquimbite [$Fe_2(SO_4)_3 \cdot 9H_2O$], *Am. Mineral.*, *94*(11–12), 1620–1628, doi:10.2138/am.2009.3179.

Altheide, T. S., V. Chevrier, C. Nicholson, and J. Denson (2009), Experimental investigation of the stability and evaporation of sulfate and chloride brines on Mars, *Earth Planet. Sci. Lett.*, *282*, 69–78, doi:10.1016/j.epsl.2009.03.002.

Arvidson, R. E., F. Poulet, J.-P. Bibring, M. Wolff, A. Gendrin, R. V. Morris, J. J. Freeman, Y. Langevin, N. Mangold, and G. Bellucci (2005), Spectral reflectance and morphologic correlations in eastern Terra Meridiani, Mars, *Science*, *307*(5715), 1591–1594, doi:10.1126/science.1109509.

Chevrier, V., and T. S. Altheide (2008), Low temperature aqueous ferric sulfate solutions on the surface of Mars, *Geophys. Res. Lett.*, *35*, L22101, doi:10.1029/2008GL035489.

Chipera, S. J., and D. T. Vaniman (2007), Experimental stability of magnesium sulfate hydrates that may be present on Mars, *Geochim. Cosmochim. Acta*, *71*, 241–250, doi:10.1016/j.gca.2006.07.044.

Chou, I-M., and R. R. Seal II (2003), Determination of epsomite-hexahydrite equilibria by the humidity-buffer technique at 0.1 MPa with implications for phase equilibria in the system $MgSO_4$-H_2O, *Astrobiology*, *3*, 619–630, doi:10.1089/153110703322610708.

Chou, I-M., and R. R. Seal II (2007), Magnesium and calcium sulfate stabilities and the water budget of Mars, *J. Geophys. Res.*, *112*, E11004, doi:10.1029/2007JE002898.

Chou, I-M., R. R. Seal II, and B. S. Hemingway (2002), Determination of melanterite-rozenite and chalcanthite-bonattite equilibria by humidity measurements at 0.1 MPa, *Am. Mineral.*, *87*, 108–114.

Fortes, A. D., I. G. Wood, M. Alfredsson, L. Vocadlo, and K. Knight (2006), The thermoelastic properties of $MgSO_4 \cdot 7D_2O$ (epsomite) from powder neutron diffraction and ab initio calculation, *Eur. J. Mineral.*, *18*, 449–462, doi:10.1127/0935-1221/2006/0018-0449.

Freemen, J. J., and A. Wang (2009), Hydrated magnesium sulfates below 0°C: Stable phases and polymorphs, *Lunar Planet. Sci.* [CD-ROM], *XXXX*, Abstract 2301.

Freemen, J. J., A. Wang, and B. L. Jolliff (2007a), Pathways to form kieserite from epsomite at mid-low temperatures, *Lunar Planet. Sci.* [CD-ROM], *XXXVIII*, Abstract 1298.

Freemen, J. J., A. Wang, and B. L. Jolliff (2007b), $MgSO_4 \cdot 11H_2O$: Powder XRD, Raman, and VIS-NIR spectroscopic characterization, *Lunar Planet. Sci.* [CD-ROM], *XXXVIII*, Abstract 1197.

Gendrin, A., et al. (2005), Sulfates in Martian layered terrains: The OMEGA/Mars Express view, *Science*, *307*(5715), 1587–1591, doi:10.1126/science.1109087.

Golden, D. C., D. W. Ming, R. V. Morris, and S. A. Mertzman (2005), Laboratory-simulated acid-sulfate weathering of basaltic materials: Implications for formation of sulfates at Meridiani Planum and Gusev Crater, Mars, *J. Geophys. Res.*, *110*, E12S07, doi:10.1029/2005JE002451.

Golden, D. C., D. W. Ming, R. V. Morris, and T. G. Graff (2008), Hydrothermal synthesis of hematite spherules and jarosite: Implications for diagenesis and hematite spherule formation in sulfate outcrops at Meridiani Planum, Mars, *Am. Mineral.*, *93*, 1201–1214, doi:10.2138/am.2008.2737.

Greenspan, L. (1977), Humidity fixed points of binary saturated aqueous solution, *J. Res. Natl. Bur. Stand., Sect. A*, *81*, 89–96.

Grevel, K. D., and J. Majzlan (2009), Internally consistent thermodynamic data for magnesium sulfate hydrates, *Geochim. Cosmochim. Acta*, *73*, 6805–6815, doi:10.1016/j.gca.2009.08.005.

Haar, L., J. S. Gallagher, and G. S. Kell (1984), *NBS/NRC Steam Tables*, Hemisphere, New York.

Head, J. W., et al. (2005), Tropical to mid-latitude snow and ice accumulation, flow and glaciation on Mars, *Nature*, *434*, doi:10.1038/nature03359.

Kieffer, H. H., T. Z. Martin, A. R. Peterfreund, B. M. Jakosky, E. D. Miner, and F. D. Palluconi (1977), Thermal and albedo mapping of Mars during the Viking primary mission, *J. Geophys. Res.*, *82*, 4249–4291, doi:10.1029/JS082i028p04249.

Kong, W. G., A. Wang, J. J. Freeman, and P. S. Sobron (2010), A comprehensive spectroscopic study of synthetic Fe^{2+}, Fe^{3+}, Mg^{2+}, Al^{3+} copiapite by Raman, XRD, LIBS, and VIS-NIR, *J. Raman Spectrogr.*, *45*, 1120–1129, doi:10.1002/jrs.2790.

Kong, W. G., A. Wang, and I-M. Chou (2011), Determination of phase boundary between kornelite and pentahydrated ferric sulfate by humidity buffer technique and Raman spectroscopy at 0.1 Mpa, *Chem. Geol.*, *284*, 333–338, doi:10.1016/j.chemgeo.2011.03.014.

Landis, J. A., and MER Athena Science Team (2007), Observation of frost at the equator on Mars by the Opportunity rover, *Lunar Planet. Sci.* [CD-ROM], *XXXVIII*, Abstract 2423.

Lichtenberg, K. A., R. E. Arvidson, S. Murchie, L. H. Roach, J. Andrews-Hanna, E. Noe Dobrea, and J. Mustard (2008), Structural and geologic relationships between igneous rocks and their alteration products in Xanthe Terra, Mars, *Proc. Lunar Planet. Sci. Conf., 39th*, Abstract 1390.

Lichtenberg, K. A., et al. (2010), Stratigraphy of hydrated sulfates in the sedimentary deposits of Aram Chaos, Mars, *J. Geophys. Res.*, *115*, E00D17, doi:10.1029/2009JE003353.

Ling, Z. C., and A. Wang (2010), A systematic spectroscopic study of eight hydrous ferric sulfates relevant to Mars, *Icarus*, *209*, 422–433, doi:10.1016/j.icarus.2010.05.009.

Ling, Z. C., A. Wang, B. L. Jolliff, R. E. Arvidson, and H. R. Xia (2008), A new phase of hydrated ferric sulfates, lausenite?, paper presented at the 8th International Conference on Raman Spectroscopy Applied to the Earth Sciences, Univ. of Ghent, Ghent, Belgium.

Ling, Z. C., A. Wang, and C. L. Li (2009), Comparative spectroscopic study of three ferric sulfates: Kornelite, lausenite and pentahydrate, *Lunar Planet. Sci.* [CD-ROM], *XXXX*, Abstract 1867.

Lipiński, I. E., J. Kuriata, I. Natkaniec, and A. Pawlokojć (2001), Neutron scattering study of sodium ammonium sulfate dihydrate, *Phys. Status Solidi B*, *227*, 477–483, doi:10.1002/1521-3951(200110)227:2<477::AID-PSSB477>3.0.CO;2-0.

Majzlan, J., and R. Michallik (2007), The crystal structure, solid solutions and infrared spectra of copiapite-group minerals, *Mineral. Mag.*, *71*(5), 553–569, doi:10.1180/minmag.2007.071.5.553.

Majzlan, J., R. Stevens, J. Boerio-Goates, B. F. Woodfield, A. Navrotsky, P. C. Burns, M. K. Crawford, and T. G. Amos (2004), Thermodynamic properties, low-temperature heat capacity anomalies, and single crystal X-ray refinement of hydronium jarosite, $(H_3O)Fe_3(SO_4)_2(OH)_6$, *Phys. Chem. Miner.*, *31*, 518–531, doi:10.1007/s00269-004-0405-z.

Majzlan, J., C. Botez, and P. W. Stephens (2005), The crystal structures of synthetics $Fe_2(SO_4)_3(H_2O)_5$ and the type specimen of lausenite, *Am. Mineral.*, *90*(2–3), 411–416, doi:10.2138/am.2005.1701.

Majzlan, J., A. Navrotsky, R. B. McCleskey, and C. N. Alpers (2006), Thermodynamic properties and crystal structure refinement of ferricopiapite, coquimbite, rhomboclase, and $Fe_2(SO_4)_3(H_2O)_5$, *Eur. J. Mineral.*, *18*(2), 175–186, doi:10.1127/0935-1221/2006/0018-0175.

Mason, B. J. (1971), *The Physics of Clouds*, 671 pp., Clarendon, Oxford, U. K.

McCord, T. B., T. M. Orlando, G. Teeter, G. B. Hansen, M. T. Sieger, N. G. Petrik, and L. V. Keulen (2001), Thermal and radiation stability of the hydrated salt minerals epsomite, mirabilite, and natron under Europa environmental conditions, *J. Geophys. Res.*, *106*, 3311–3319, doi:10.1029/2000JE001282.

Mellon, M. T., W. C. Feldman, and T. H. Prettyman (2004), The presence and stability of ground ice in the southern hemisphere of Mars, *Icarus*, *169*, 324–340, doi:10.1016/j.icarus.2003.10.022.

Milliken, R. E., K. S. Edgett, G. Swayze, R. N. Clark, B. J. Thomson, R. Anderson, and J. F. Bell III (2009), Clay and sulfate-bearing rocks in a stratigraphic sequence in Gale Crater, *Proc. Lunar Planet. Sci. Conf., 40th*, Abstract 1479.

Murchie, S., et al. (2007), CRISM mapping of layered deposits in western Candor Chasma, Abstract 3238 presented at the Seventh International Conference on Mars, Lunar and Planet. Inst., Pasadena, Calif.

Murchie, S. L., et al. (2009), Compact reconnaissance imaging spectrometer for Mars investigation and data set from the Mars Reconnaissance Orbiter's primary science phase, *J. Geophys. Res.*, *114*, E00D07, doi:10.1029/2009JE003344.

Peng, Z. X., A. Wang, and B. L. Jolliff (2010), Hydrothermal process on Mars—Mission observations and a laboratory simulation experiment, *Lunar Planet. Sci.* [CD-ROM], *XXXXI*, Abstract 2586.

Peterson, R. C., and R. Wang (2006), Crystal molds on Mars: Melting of a possible new mineral species to create Martian chaotic terrain, *Geology*, *34*, 957–960, doi:10.1130/G22678A.1.

Roach, L., et al. (2007), Magnesium and iron sulfate variety and distribution in East Candor and Capri Chasma, Valles Marineris, Abstract 3223 presented at the Seventh International Conference on Mars, Lunar and Planet. Inst., Pasadena, Calif.

Roach, L., J. F. Mustard, S. L. Murchie, J.-P. Bibring, R. E. Arvidson, J. L. Bishop, R. E. Milliken, F. Seelos, and the CRISM Science Team (2008), Constraints on the rate of sulfate phase changes in Valles Marineris interior layered deposits, *Proc. Lunar Planet. Sci. Conf., 39th*, Abstract 1823.

Roach, L., J. F. Mustard, S. L. Murchie, J. L. Bishop, B. L. Ehlmann, K. Lichtenberg, M. Parente, and the CRISM Science Team (2009a), Sulfate and hematite stratigraphy in Capri Chasma, Valles Marineris, *Proc. Lunar Planet. Sci. Conf., 40th*, Abstract 1826.

Roach, L. H., J. F. Mustard, S. L. Murchie, J.-P. Bibring, F. Forget, K. W. Lewis, O. Aharonson, M. Vincendon, and J. L. Bishop (2009b), Testing evidence of recent hydration state change in sulfates on Mars, *J. Geophys. Res.*, *114*, E00D02, doi:10.1029/2008JE003245.

Roach, L. H., J. F. Mustard, G. Swayze, R. E. Milliken, J. L. Bishop, S. L. Murchie, and K. Lichtenberg (2010), Hydrated mineral stratigraphy of Ius Chasma, Valles Marineris, *Icarus*, *206*, 253–268, doi:10.1016/j.icarus.2009.09.003.

Schofield, J. T., J. R. Barnes, D. Crisp, R. M. Haberle, S. Larsen, J. A. Magalhaes, J. R. Murphy, A. Seiff, and G. Wilson (1997), The Mars Pathfinder atmospheric structure investigation meteorology (ASI/MET) experiment, *Science*, *278*(5344), 1752–1758, doi:10.1126/science.278.5344.1752.

Smith, M. D. (2002), The annual cycle of water vapor on Mars as observed by the thermal emission spectrometer, *J. Geophys. Res.*, *107*(E11), 5115, doi:10.1029/2001JE001522.

Smith, M. D., et al. (2004), First atmospheric science results from the Mars Exploration Rovers Mini-TES, *Science*, *306*(5702), 1750–1753, doi:10.1126/science.1104257.

Smith, M. D., M. J. Wolff, N. Spanovich, A. Ghosh, D. Banfield, P. R. Christensen, G. A. Landis, and S. W. Squyres (2006), One Martian year of atmospheric observations using MER Mini-TES, *J. Geophys. Res.*, *111*, E12S13, doi:10.1029/2006JE002770.

Spanovich, N., M. D. Smith, P. H. Smith, M. J. Wolff, P. R. Christensen, and S. W. Squyres (2006), Surface and near-surface atmospheric temperatures for the Mars Exploration Rover landing sites, *Icarus*, *180*, 314–320, doi:10.1016/j.icarus.2005.09.014.

Suleimenov, O. M., M. Y. Zolotov, and I. L. Khodakovsky (1986), Stability of salt hydrates in Martian regolith, *Lunar Planet. Sci.*, *XVII*, 845–846.

Tosca, N. J., and S. M. McLennan (2006), Chemical divides and evaporite assemblages on Mars, *Earth Planet. Sci. Lett.*, *241*, 21–31, doi:10.1016/j.epsl.2005.10.021.

Tosca, N. J., S. M. McLennan, D. Lindsley, and M. Schoonen (2004), Acid-sulfate weathering of synthetic Martian basalt: The acid-fog model revisited, *J. Geophys. Res.*, *109*, E05003, doi:10.1029/2003JE002218.

Tosca, N. J., A. Smirnov, and S. M. McLennan (2007), Application of the Pitzer ion interaction model to isopiestic data for the $Fe_2(SO_4)_3$–H_2SO_4–H_2O system at 298.15 and 323.15 K, *Geochim. Cosmochim. Acta*, *71*, 2680–2698, doi:10.1016/j.gca.2007.03.020.

Tosca, N. J., S. M. McLennan, M. D. Dyar, E. C. Sklute, and F. M. Michel (2008), Fe oxidation processes at Meridiani Planum and implications for secondary Fe mineralogy on Mars, *J. Geophys. Res.*, *113*, E05005, doi:10.1029/2007JE003019.

Vaniman, D. T., and S. J. Chipera (2006), Transformation of Mg- and Ca-sulfate hydrates in Mars regolith, *Am. Mineral.*, *91*, 1628–1642, doi:10.2138/am.2006.2092.

Vaniman, D. T., D. L. Bish, S. J. Chipera, C. I. Fialips, J. W. Carey, and W. C. Feldman (2004), Magnesium sulphate salts and the history of water on Mars, *Nature*, *431*, 663–665, doi:10.1038/nature02973.

Wang, A., and Z. C. Ling (2011), Ferric sulfates on Mars: A combined mission data analysis of salty soils at Gusev Crater and laboratory experimental investigations, *J. Geophys. Res.*, *116*, E00F17, doi:10.1029/2010JE003665.

Wang, A., J. J. Freeman, B. L. Jolliff, and I-M. Chou (2006), Sulfates on Mars: A systematic Raman spectroscopic study of hydration states of magnesium sulfates, *Geochim. Cosmochim. Acta*, *70*, 6118–6135, doi:10.1016/j.gca.2006.05.022.

Wang, A., J. J. Freeman, and B. L. Jolliff (2007), Formation rate of amorphous magnesium sulfates at low temperatures approaching the current surface conditions on Mars, *Lunar Planet. Sci.* [CD-ROM], *XXXVIII*, Abstract 1195.

Wang, A., et al. (2008), Light-toned salty soils and coexisting Si-rich species discovered by the Mars Exploration Rover Spirit in Columbia Hills, *J. Geophys. Res.*, *113*, E12S40, doi:10.1029/2008JE003126.

Wang, A., J. J. Freeman, and B. L. Jolliff (2009), Phase transition pathways of the hydrates of magnesium sulfate in the temperature range 50°C to 5°C: Implication for sulfates on Mars, *J. Geophys. Res.*, *114*, E04010, doi:10.1029/2008JE003266.

Wang, A., Z. C. Ling, and J. J. Freeman (2010), Stability fields and phase transition pathways of ferric sulfates in 50°C to 5°C temperature range, *Lunar Planet. Sci.* [CD-ROM], *XXXXI*, Abstract 2303.

Zolotov, M. Y. (1989), Water-bearing minerals in the Martian soil (thermodynamic prediction of stability), *Lunar Planet. Sci.*, *XX*, 1257–1258.

Zolotov, M. Y., and M. Mironenko (2007), Timing of acid weathering on Mars: A kinetic-thermodynamic assessment, *J. Geophys. Res.*, *112*, E07006, doi:10.1029/2006JE002882.

I.-M. Chou, U.S. Geological Survey, 954 National Center, Reston, VA 20192, USA.

J. J. Freeman, B. L. Jolliff, and A. Wang, Department of Earth and Planetary Sciences, Washington University in St. Louis, St. Louis, MO 63130, USA. (alianw@levee.wustl.edu)